Geophys. J. Int. (1999) **136,** 19–40

Shear heating in continental strike-slip shear zones: model and field examples

Philippe Hervé Leloup,[1] Yannick Ricard,[2] Jean Battaglia[1] and Robin Lacassin[1]

[1] *Laboratoire de tectonique et mécanique de la lithosphère,* CNRS-UMR 7578, *Institut de physique du globe de Paris,* 4 *place Jussieu,* 75252 *Paris cedex* 05, *France*

[2] *Laboratoire de Sciences de la Terre,* URA 726, *Ecole Normale Supérieure de Lyon,* 46 *allée d'Italie,* 69364 *Lyon cedex* 07, *France*

Accepted 1998 July 6. Received 1998 June 21; in original form 1998 February 24

SUMMARY

A two-layer (crust and upper mantle), finite di erence steady-state thermomechanical model of a long-lived (several million years) lithospheric strike-slip fault is presented, and its predictions compared with field observations from various major fault zones. In order to estimate the maximum amount of shear heating, all mechanical energy is assumed to be dissipated in heat, in ductile as well as in brittle layers. Deformation follows a friction law in the brittle layer(s), and a power-flow law in the ductile one(s). Variations of several independent parameters and their influence on the thermomechanical state of the fault zone and on shear heating are systematically explored. Shear heating is found to be more important in fault zones a ecting an initially cold lithosphere, and increases with slip rate, friction coe cient and sti ness of materials. In extreme cases (slip rate of 10 cm yr^{-1}, sti lithosphere), shear heating could lead to temperature increases close to 590 °C at the Moho, and 475 °C at 20 km depth. For more common cases, shear heating leads to smaller temperature increases, but can still explain high-grade metamorphic conditions encountered in strike-slip shear zones. However, modelled temperature conditions often fall short of those observed. This could be due to heat transport by mechanisms more e cient than conduction. Common syntectonic emplacement of granitic melts in ductile strike-slip shear zones can be explained by lower crust partial melting induced by shear heating in the upper mantle. Besides slip rate, the possibility of such melting depends mostly on the upper mantle rheology and on the fertility of the lower crust: for hard upper mantle and highly fertile lower crust, partial melting could occur at rates of 1 cm yr^{-1}, while in most cases it would result from the breakdown of micas for slip rates over 3 cm yr^{-1}. As a result of shear heating, partial melting of the upper mantle could occur in the presence of small amounts of fluids. Rise of magmas and/or hot fluids in the shear zone will further enhance the temperature increase in shallower parts of the fault zone. In nature, shear heating would inevitably cause strain localization in the deeper parts of strike-slip faults, as is often observed in the field for crustal shear zones.

Key words: crustal deformation, fault models, finite di erence methods, heat flow, lithospheric deformation, tectonics.

1 INTRODUCTION

Prograde metamorphism is due to temperature increase resulting from four main possible causes: deep burial of rocks, rise of regional or local heat flow, thickening of radioactive-rich crust, and shear heating. Most metamorphic rocks crop out in collision belts where all these processes may have acted together, making the importance of each one di cult to decipher. In particular, the e ciency of shear heating (or strain heating) is a subject of debate. While shear heating has long been considered a major heat source by field geologists (e.g. Nicolas *et al.* 1977) and by some geophysicists (e.g. Scholz 1980; Barr & Dahlen 1989; Molnar & England 1990), theoretical calculations suggest that it is unlikely to be of prime importance (Brun & Cobbold 1980; Fleitout & Froidevaux 1980). Indeed, when a rock produces heat by friction, it necessarily becomes warmer and softer, a phenomenon that bu ers the heat production.

In this debate, metamorphism associated with major strike-slip faults is of particular interest, as burial of rocks, heat-flow regional increase, and crustal thickening are limited for such faults. Field observations along continental strike-slip shear

zones have provided direct evidence of high temperatures and/or partial melting at moderate depth (e.g. Nicolas *et al.* 1977; Scholz *et al.* 1979; Leloup & Kienast 1993; Tommasi *et al.* 1994; Leloup *et al.* 1995). These observations raise the question of whether strike-slip shear zones only channel hot fluids and/or plutons produced by an external heat source, or if they can produce enough heat by friction to raise temperatures substantially and generate *in situ* magmas. Previous quantitative estimates of shear heating along strike-slip faults led to the conclusion that shear heating could not usually increase temperature by more than 200 °C, nor provoke partial melting unless in layered structures with contrasted rheology (Fleitout & Froidevaux 1980). As the lithosphere is fundamentally composed of two such layers (crust and upper mantle), Ricard, Froidevaux & Hermance (1983) developed a finite di erence model with a quartzitic crust and an olivine-rich upper mantle to evaluate shear heating along a translithospheric strike-slip fault. The aim of the present paper is to explore the influence of various parameters on the temperature produced by shear in an updated version of this model. These parameters are the lithospheric thermal conductivity, the fault slip rate, the rock rheologies, the basal heat flow, the radioactive heat production and the Moho depth. The main characteristic of our model is to consider shear heating in the whole lithosphere, for both brittle and ductile deformations. Our final goal is to estimate what plausible maximum temperatures can be reached and to compare these results with metamorphic conditions observed along major strike-slip shear zones.

2 NUMERICAL MODEL

2.1 Calculation procedure

Following Ricard *et al.* (1983) we use 2-D steady-state numerical models that calculate the heat production by shear along a vertical strike-slip fault and resulting temperatures in a section perpendicular to the fault. We choose to calculate steady-state solutions for two reasons. First, computation of time-dependent solutions would require the precise knowledge of the whole kinematic history of each fault, which is never the case. Second, in the crust and along the fault, steady state is rapidly reached (after some millions of years, see Section 2.3.3). The fault is vertical, infinitely long and strikes parallel to the y-axis (Fig. 1). Motion is purely horizontal. Because shear heating is symmetrical with respect to the fault and because all variables (conductivity, rock rheology, radioactive heat production, etc.) are constant at a given depth, we solve the problem in the xz-plane on one side of the fault only (Fig. 1). The left, the upper and the lower limits of the grid correspond to the fault, the earth surface and the lithosphere/asthenosphere boundary, respectively. Mohorovicic discontinuity (Moho) is represented by a horizontal boundary at depth M_z, which separates rocks of contrasting rheologies (Fig. 1). Our two main assumptions are that (1) the fault rate is constant and a thermal steady state is reached, and (2) all the mechanical energy is dissipated by heat. Most calculations were performed on a grid containing 40×40 (1600) elements, each 5 km wide and 2.5 km high (Fig. 1).

We tested two distinct numerical models. The first one should give a more precise solution, as it does not postulate any other assumption than (1) and (2) above, solving eqs (4), (5), (7) and (11) mentioned below. However, in this case, the depth of the brittle/ductile transition (z b/d) was arbitrarily fixed before calculation. The second model is a simplified one, where we consider deformation, and hence shear heating, only on vertical planes parallel to the main fault, thus solving eqs (6), (8) and (11) given below. In this second case, the depth of the brittle/ductile transition is calculated during the iterative process that leads to the final solution. Each iteration is divided into three successive steps.

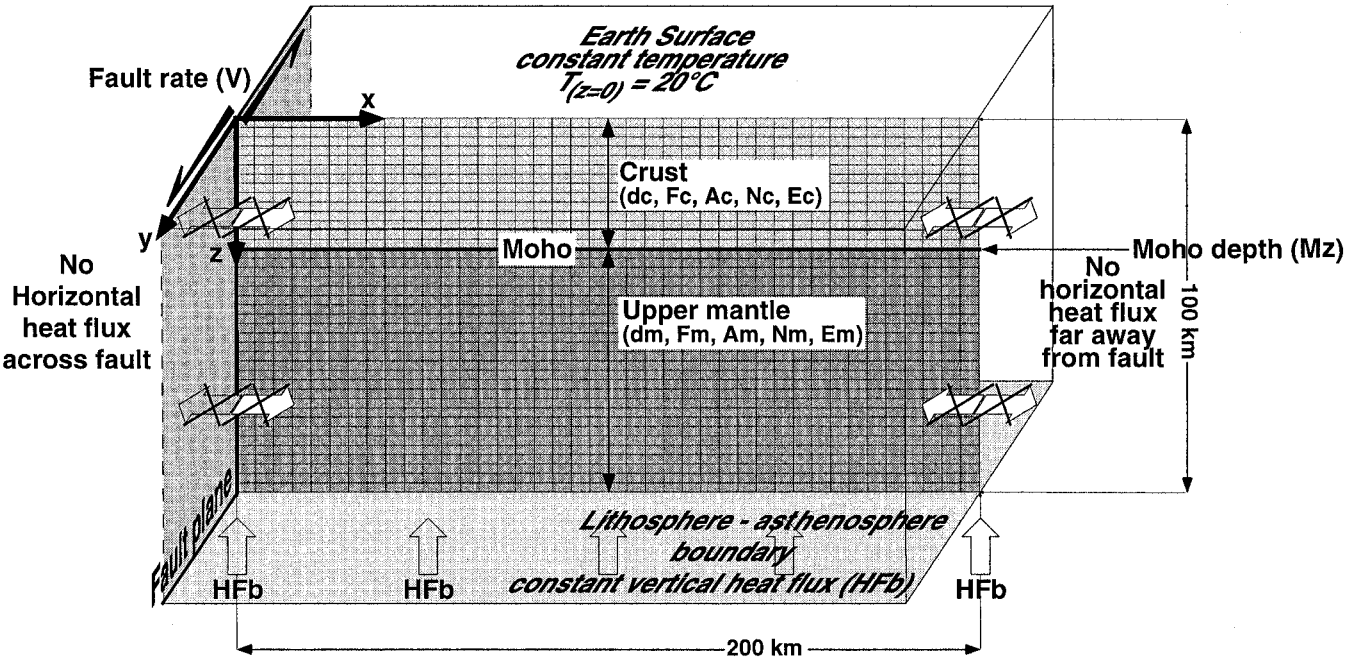

Figure 1. Numerical model characteristics. Abbreviations are detailed in Table 1. See text for details.

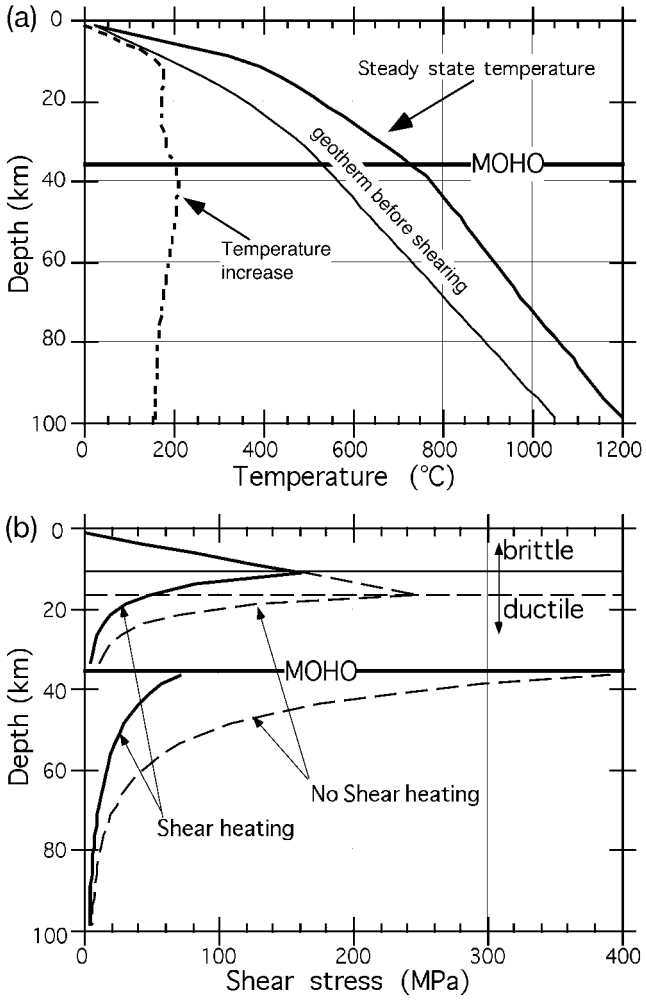

Figure 2. Vertical variations of temperature and shear stress along the fault for reference parameters (bold numbers in Table 1). (a) Temperature profiles before and during shearing, and corresponding temperature increase. (b) Shear-stress profile during shearing in the case of shear heating (continuous line) and no shear heating (long-dashed line). The peak in shear stress is located either in the last grid element above, or in the first below, the brittle/ductile transition.

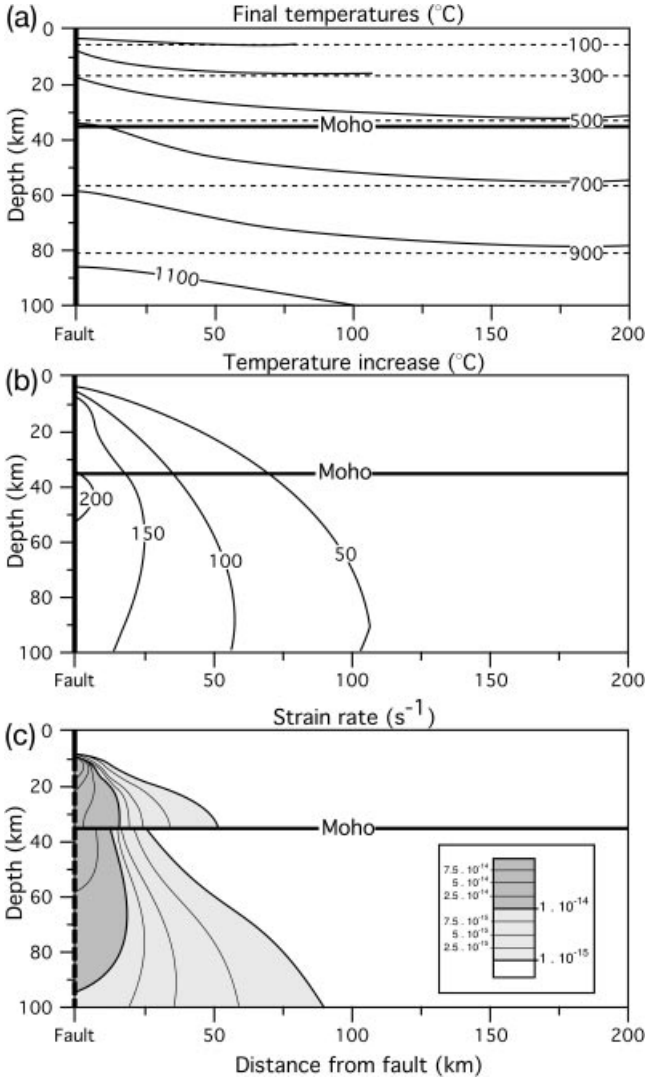

Figure 3. Temperatures, strain rates and frictional heat production for reference parameters (bold numbers in Table 1) in a vertical half-space perpendicular to the fault. (a) Isotherms during shearing (continuous lines) compared to initial ones (dashed lines). (b) Temperature increase due to shear heating. Note that temperatures mostly increase along the fault near the brittle/ductile transition and in the upper mantle. (c) Shear strain in ductile layers.

(1) Given 'initial' temperatures, a strength profile is calculated: at a given depth, the deformation mechanism (brittle or ductile) is assumed to be the one for which the shear stress on the fault is the lowest.

(2) When the depth of the brittle/ductile transition has been determined, shear heating is calculated as a function of depth, applying a friction law for the brittle part of the fault and a power-flow law for its ductile part.

(3) Knowing both this frictional heat production and the radiogenic heat production, the heat di usion equation is solved to calculate 'new' temperatures.

We iterate these three steps until temperatures do not evolve significantly between successive calculations, implying that a steady-state solution has been found. Vertical profiles of temperature, temperature increase and shear stress are drawn (Fig. 2), together with 'maps' of temperatures and temperature increases in vertical cross-sections perpendicular to the fault (Fig. 3). Temperature increases are calculated with respect to a normal geotherm computed without shear heating (Fig. 2a). Basic formulae used for calculation are detailed in the following paragraphs.

The di erences between the full and simplified solutions are discussed in Appendix A. As the predicted temperature increases near the fault di er by less than 10 per cent and final temperatures by less than 5 per cent, we present in this paper simplified solutions, where the depth of the brittle/ductile transition is calculated, not imposed.

2.2 Boundary conditions and parameters

As the fault is strike slip, there is no vertical motion. Horizontal motion of velocity $V/2$ along the y-axis is imposed on the right side of the computation box and in the brittle layer, while the fault itself stays fixed. The resultant initial velocity field consists of two rigid blocks separated by the fault in the brittle

layer (relative velocity on the fault is V), and a continuous velocity field in the ductile layer (total relative velocity between boundaries is V). At large depth, the horizontal velocity becomes a function of x only ($\partial v/\partial z = 0$ is imposed at $z = 100$ km). After calculation, ductile deformation is mostly localized in a shear zone, with a half-width of less than 25 km (see below). Such localization is achieved more quickly if an initial Gaussian-shaped temperature perturbation, of a few tenths of a degree, is imposed in the initial temperature distribution. Such boundary conditions imply that far-field forces of plate-tectonic type (generated outside the model box) are driving the fault kinematics.

A constant temperature of 20 °C is maintained at the top boundary of the grid (earth's surface, Figs 1, 2a and 3b). By symmetry, horizontal heat flow across the fault is null (Fig. 1). We assume that shear-heating e ects are negligible more than 200 km away from the fault, implying that heat flow across a vertical boundary at $x = 200$ km is negligible (Fig. 1). Heat flow at the base of the lithosphere ($z = 100$ km) is constant and equal to HFb (Fig. 1).

Besides HFb, 14 other parameters are fixed for each run (Table 1). Three of these parameters define general characteristics of the model: the fault slip rate (V), the thermal conductivity (K), and the Moho depth (M_z). Five parameters define the rheology of each layer. The density (ρ), and the friction coe cient (F) allow us to calculate the friction law when the material is brittle. The pre-exponent constant (A), the power-flow-law exponent (N), and the activation energy (E) define a power-flow law when rocks deform ductilely (see below). The last parameter is the radioactive heat production per unit time and volume (Q_r), which is depth-dependent.

2.3 Main governing equation

2.3.1 Strength profile

Along the fault, in the brittle zone, it is assumed that the Coulomb criterion for failure is reached:

$$\tau_b \approx F\sigma_n, \tag{1}$$

where F is the friction coe cient, and τ_b and σ_n are the shear and normal stresses, respectively. σ_n is assumed to be close to lithostatic stress. τ_b thus increases with depth as a function of the weight of the overlying rocks.

At a depth z,

$$\tau_{b(z)} = Fg \int_0^z \rho(u)\, du, \tag{2}$$

where g is the gravity acceleration ($g \approx 9.8$ m s^{-2}) and $\rho(z)$ the depth-dependent density.

On the other hand, in the viscous layer, the deformation is a function of both x and z, and the shear stresses τ_{xy} and τ_{yz} are non-zero:

$$\frac{\partial \tau_{xy}}{\partial x} + \frac{\partial \tau_{yz}}{\partial z} = 0. \tag{3}$$

Following experimental results, and thus assuming a non-linear law of deformation of the form $\dot{\varepsilon} = A\tau^N \exp(-E/RT)$ between deviatoric stresses and strain rate (e.g. Weertman 1978), one writes

$$\frac{\partial V}{\partial x} = A(\tau_{xy}^2 + \tau_{yz}^2)^{(N-1)/2} \tau_{xy} \exp(-E/RT) \tag{4}$$

and

$$\frac{\partial V}{\partial z} = A(\tau_{xy}^2 + \tau_{yz}^2)^{(N-1)/2} \tau_{yz} \exp(-E/RT). \tag{5}$$

In the two previous equations, V is the velocity along the y-axis, T the temperature, E the activation energy of ductile deformation, N the power-law exponent, A the pre-exponent constant, and R the universal gas constant ($R = 8.32$ J mol^{-1} K^{-1}). In the Appendix, we show how to solve these equations coupled with the equation of heat conservation.

It seems obvious, however, that the mechanical behaviour is dominated by shear on vertical planes parallel to the main fault ($\tau_{xy} \neq 0$) rather than by shear on the horizontal plane ($\tau_{yz} \approx 0$). In this case, by integration of (4) one derives the

Table 1. Thermal and mechanical parameters.

Parameter	Abbreviation	unit	range
Thermal parameters			
Thermal conductivity	K	W m^{-1} K^{-1}	1.5–**2.5**–4
Basal heat flow	HFb	mW m^{-2}	10–**20**–30
Crust radioactive heat production	Q_r	mW m^{-3}	0–**1**–2
Moho Depth	M_z	km	25–**35**–60
Mechanical parameters			
Slip rate	V	cm yr^{-1}	0–**3**–10
Crust density	ρc	kg m^{-3}	**2800**
Upper mantle density	ρm	kg m^{-3}	**3200**
Crust friction coe cient	Fc	dimensionless	0.001–**0.6**–0.85
Upper mantle friction coe cient	Fm	dimensionless	0.001–**0.6**–0.85
Power flow law coefficients	**pre-exponent constant:** A [Pa^{-N} s^{-1}]	**exponent:** N [dimensionless]	**activation energy: E** [10^5 J mol^{-1}]
Crust	Ac	Nc	Ec
soft: Westerly granite (wet)	7.962 10^{-16}	1.9	1.4
average: Westerly granite (dry)	**3.16 10^{-26}**	**3.3**	**1.86**
hard: orthopyroxenite (dry)	1.26 10^{-15}	2.4	2.93
Upper mantle	Am	Nm	Em
soft: Anita bay dunite	7.94 10^{-17}	3.35	4.44
average: Mt Burnet dunite (wet)	**7.94 10^{-34}**	**5.1**	**3.92**
hard: dunite (dry)	7.94 10^{-18}	3.6	5.35

simplified equation

$$\tau_{d(z)} = \tau_{xy} = \left(V \Big/ 2 \int_0^{\infty} \exp\left(- \frac{E}{RT(u, z)} \right) du \right)^{1/N}. \quad (6)$$

The errors introduced by this approximation are discussed in the Appendix.

By plotting $\tau_{d(z)}$ and $\tau_{b(z)}$ as a function of depth, one obtains a lithospheric strength profile (Fig. 2b). At a given depth, the relevant deformation mechanism is the one for which the shear stress is minimum (e.g. Goetze & Evans 1979; Brace & Kohlstedt 1980).

2.3.2 *Heat production*

One of the two basic assumptions of the model is that all mechanical energy is dissipated in heat (Joule 1850). The heat produced by shear per unit time and volume (Q in [W m^{-3}]) is simply given by

$$Q_f = \tau_{xy} \frac{\partial V}{\partial x} + \tau_{yz} \frac{\partial V}{\partial z}. \quad (7)$$

Here again, as discussed in the Appendix, we assume that most of the heat is produced by shear heating along vertical planes. Eq. (7) simplifies to

$$Q_f = \tau_{xy} \frac{\partial V}{\partial x}. \quad (8)$$

If $\tau_{d(z)} > t_{b(z)}$ we assume that rocks deform brittlely. Heat production is localized along the fault plane (first column of the grid) and only half of this heat di uses in each side. Therefore (8) becomes

$$Q_{f(x=0,z)} = \tau_{b(z)} \frac{V}{2l}, \quad (9)$$

where l is the width along the x-axis of the considered unit cell.

If $\tau_{d(z)} < t_{b(z)}$ rocks deform ductilely and heat is produced wherever the deformation takes place. Consequently, (8) leads to

$$Q_{f(x,z)} = A \tau_{d(z)}^{N+1} \exp(-E/RT_{(x,z)}). \quad (10)$$

Although no localization of deformation is imposed within the ductile shear zone, steady-state solutions show a strong localization of deformation and heat production. In the ductile shear zone, strain rates are maximum below the brittle fault and decrease by one order of magnitude in a zone of half-width $\approx$20 km (Fig. 3c). Such strain localization in the ductile layer is explained by shear heating: a slight temperature increase, for example due to the proximity of localized brittle deformation, leads to higher strain rates inducing more shear heating that contributes to raising the temperature even further. Consequently, maximum ductile shear heating takes place in the centre of the shear zone and becomes negligible less than 80 km away from the fault.

Heat is also produced by radioactive decay in an amount $Q_r(z)$ defined by a radioactive heat production profile chosen for each run.

2.3.3 *Heat diffusion*

If the thermal conductivity is everywhere given by K, the steady-state heat conduction is

$$\nabla^2 T + \frac{Q_f + Q_r}{K} = 0. \quad (11)$$

We approximate (11) by a finite di erence method, calculating the 'new' temperature at any point of the grid as a function of 'old' temperatures at the four neighbouring points and of the local heat production. The solution is considered to be stable when an iteration does not change the temperature of any nodes of the grid by more than 10^{-3} °C.

Heat production by shear is maximum along the fault where shear stress is maximum: at the brittle/ductile transition (10–20 km deep) and in the uppermost mantle (Fig. 2b). A simple heat di usion scaling of the form $d = 2\sqrt{\kappa t}$ (t being the timescale necessary for heat to di use to a distance d from the heat source, and κ being the lithosphere thermal di usivity of $\approx 1\ 10^{-6}$ m^2 s^{-1}) indicates that, near the fault, heat produced by shear di uses through the crust in less than 4 Myr. The steady regime is in fact reached even more quickly, as the shear stress, and hence heat production, is greater at the beginning of deformation when temperatures are lower. Far from the fault zone and in the lower part of the lithosphere, where no heat is produced, the temperature changes slowly by di usion. In these regions, however, temperature changes are so small that metamorphism does not take place and field observations cannot constrain our modelling. In agreement with 1-D models (Fleitout & Froidevaux 1980), steady-state temperatures close to the fault, in the crust and in the upper mantle, will be reached after only a few million years of strike-slip faulting at a constant rate.

2.4 Parameter values

As many parameters (at least 15) are involved in our calculations, we decided to choose for each one a possible range of variation and a reference value (Table 1). This reference corresponds to the *a priori* most plausible values inferred from our knowledge of the lithosphere and of large continental strike-slip faults. In this way, we can explore the influence of each parameter individually: except for the one under investigation, all parameters are fixed to their reference values. Thermal conductivity, basal heat flow, radiogenic heating, and Moho depth influence the temperature structure of the lithosphere both before and during shearing: these will be referred to as thermal parameters as opposed to the mechanical ones (slip rate, friction coe cient and power law parameters) that are only important when motion takes place along the fault.

3 RESULTS

3.1 Reference model: a plausible lithospheric fault model

In the reference model all parameters are set to their reference value (Table 1). The crust is 35 km thick, with a homogeneous radioactivity of 1 mW m^{-3}, a friction coe cient of 0.6 and the power-flow law of dry Westerly granite (Hansen & Carter 1983). Mantle rocks do not show any radioactivity and have the rheology of wet Mt Burnet dunite (Post 1977). Thermal conductivity is set to 2.5 W m^{-1} K^{-1}, and basal heat flow to

20 mW m^{-2}. These parameters lead to a normal geotherm where the Moho is at 534 °C (Fig. 2a), and a surface heat flow of 53 mW m^{-2} (Fig. 2c). After motion on the fault at a rate of 3 cm yr^{-1} and consequent shear heating, isotherms are perturbed and temperature substantially increases close to the fault (Fig. 3a). For example, the temperature at the Moho reaches 735 °C in the fault zone, while it remains at 534 °C far from it (Figs 2a and 3a). Surface heat flow on the fault trace reaches 109 mW m^{-2} (Fig. 6d). Temperature mostly increases at two depths: in the crust at the brittle/ductile transition (+176 °C, ≈10 km depth), and in the mantle just below the Moho discontinuity (+208 °C) (Fig. 3b). These zones correspond to places where shear stress is maximum (Fig. 2b). Ductile deformation is localized below the main brittle fault. In the crust, the maximum strain rate is 9×10^{-14} s^{-1}, in the shear-zone centre, just below the brittle/ductile transition (Fig. 3c). Strain rates decrease by one order of magnitude less than 25 km from the left boundary of the grid. The higher strain rates ($>10^{-14}$ s^{-1}), typical of geological deformation rates, define a vertical shear zone a ecting the whole lithosphere.

3.2 Variations of thermal parameters

3.2.1 *Lithospheric average thermal conductivity*

Average conductivity for the whole crust probably ranges between 1.5 and 3 W m^{-1} K^{-1} (England & Thompson 1984). Conductivity of the lithospheric mantle is usually assumed to be equal to 3 W m^{-1} K^{-1} (Pinet *et al.* 1991; Gaudemer *et al.* 1988). We decided to take 2.5 W m^{-1} K^{-1} as the reference value for lithospheric heat conductivity and to test variations of this parameter between 1 and 4 W m^{-1} K^{-1} (Table 1).

Such variations significantly change the model by a ecting the initial thermal structure of the lithosphere. For high thermal conductivities, initial temperatures are very low (for example 340 °C at the Moho for $K = 4$ W m^{-1} K^{-1}), and the shear-heating e ect is important (+320 °C), leading to moderate final temperatures (660 °C at the Moho) (Fig. 4). On the other hand, a low thermal conductivity induces high initial temperatures (880 °C at the Moho for $K = 1.5$ W m^{-1} K^{-1}), and then a small shear heating e ect (+50 °C) and very high final temperatures (930 °C at the Moho) (Fig. 4). Extreme values of conductivity lead to thermal structures before shearing that are not realistic. Indeed, a value of $K = 4$ W m^{-1} K^{-1} would imply that low greenschist metamorphism would be barely attained in the lower crust, while for $K = 1.5$ W m^{-1} K^{-1} the whole lower crust would be at temperatures compatible with partial melting. Average lithospheric conductivity thus probably lies between 2 and 3 W m^{-1} K^{-1}.

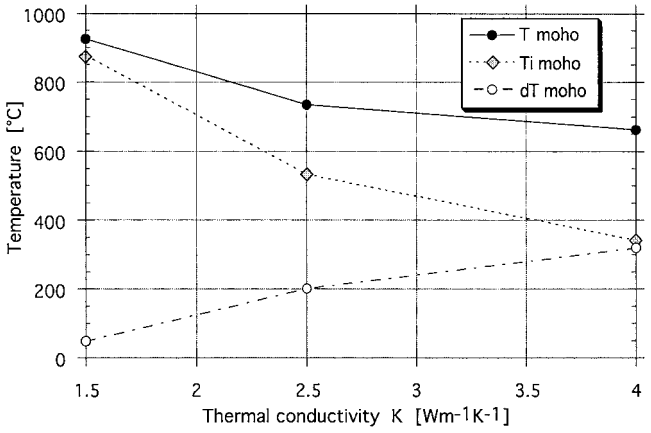

Figure 4. Influence of thermal conductivity on Moho initial temperature (Ti), temperature increase (dT) and final temperature (T) at shear zone centre. All other parameters are set to their reference values (see Table 1).

3.2.2 *Radiogenic heating and basal heat flow*

Radioactive heat production decreases with depth in the crust and is negligible in the mantle, although various radioactive heat production profiles appear consistent with the observed surface heat flow (e.g. Chapman & Furlong 1991). Radioactive heat production in amphibolite facies rocks representative of the middle crust and in granulites of the lower crust is between 1 and 1.6 mW m^{-3}, and between 0.4 and 0.45 mW m^{-3}, respectively (e.g. Pinet *et al.* 1991). A model with heat production values of 2 mW m^{-3} in the upper 10 km, 1.6 mW m^{-3} from 10 to 20 km and 0.4 mW m^{-3} for the lower crust is thus probably realistic (model 1, Fig. 5). In an attempt to simplify this crust profile we tested two alternative models: a single radioactive layer 15 km thick in which $Q_r = 2$ mW m^{-3} (model 2, Fig. 5) (England & Thompson 1984); and a homogeneous crustal heat production of 1 mW m^{-3} (model 3, Fig. 5). The choice of one of these models is not critical for the final temperatures reached along the fault, but has repercussions for the importance of shear heating (Fig. 5b). We chose model 3 as our reference heat production profile because it is simple and leads to temperatures that do not di er more than 10 per cent from model 1 (Fig. 5).

If the crustal radioactive heat production is zero, the shear-heating e ect is very important and the temperature increases by nearly 400 °C at the Moho (model 4, Fig. 5b). A uniform radioactive heat production set to 2 mW m^{-3} would produce nearly no shear-heating e ect (model 5, Fig. 5b). These results mean that a cooler lithosphere before shearing induces a larger temperature increase by shear heating, but finally reaches temperatures very close from those attained from hotter initial conditions.

Sclater *et al.* (1980) estimated the basal heat flow below continents to be between 17 and 31 mW m^{-2}. A detailed study of the Canadian and Scandinavian shields led Pinet and co-workers to estimate a basal heat flow as low as ≈10 mW m^{-2} under cratons (Pinet & Jaupart 1987; Pinet *et al.* 1991). This basal heat flow is higher in thinned areas and probably in young orogenic areas. We choose HFb = 20 mW m^{-2} as our reference value with variations between 10 and 30 mW m^{-2} (Table 1). A basal heat flow of 20 mW m^{-2}, together with a uniform crustal radioactive heat production of 1 mW m^{-3}, gives a surface heat flow of 53 mW m^{-2}, typical for continents.

A high basal heat flow obviously leads to high temperatures in the crust (Fig. 6a). But, as is the case for radioactivity, shear heating decreases sharply with increasing initial temperature, bu ering final temperatures. Crustal temperatures along the fault after shearing do not vary by more than 100 °C whatever the basal heat flow (Fig. 6b) and for any radioactive heat production below 1.5 mW m^{-3} (Fig. 5b).

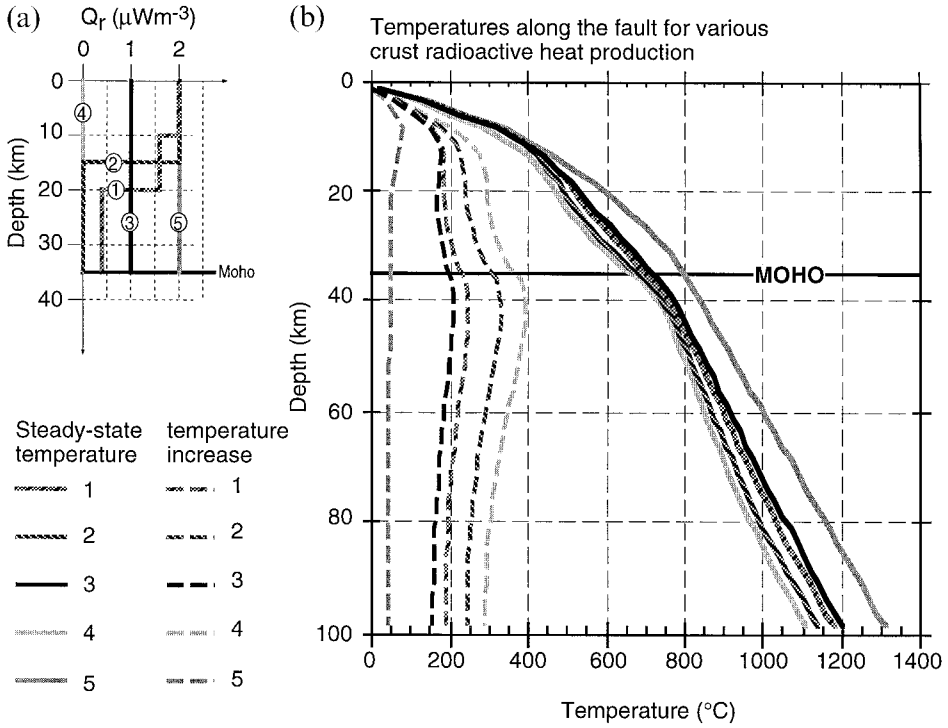

Figure 5. Influence of crustal radioactivity on thermal state. All other parameters are set to their reference values (see Table 1). (a) Proposed models for vertical distribution of radioactivity in crust. See text for details. (b) Temperature and temperature-increase profiles along the fault for proposed vertical distributions of radioactivity.

3.2.3 Moho depth

The Moho depth (M_z) influences the thermal structure as it fixes the thickness of the radioactive crust and the depth of the rheological limit (Fig. 7a). Surprisingly, when M_z varies between 20 and 45 km, the final temperature does not vary much (Fig. 7b). When the crust is thin (i.e. $M_z = 20$ km) these final temperatures are mostly due to shear heating, while in the case of a thick crust (i.e. $M_z = 45$ km) they are mostly due to radioactivity. The corresponding surface heat flows are nearly constant over the fault: ≈ 110 mW m^{-2}.

In a single-layer model (i.e. without the Moho discontinuity) the thermal structure of the lithosphere changes radically because heat production is restricted near the brittle/ductile transition. A single-layer model, with the power-law flow of the crust, and a heat production of 1 mW m^{-3} in the upper 35 km, leads to much lower temperatures in the lower crust, and a surface heat flow (105 mW m^{-2}) comparable to that of the reference model. For this single-layer model, the temperature increase at 35 km depth is only +80 °C (final temperature 615 °C), as compared with +200 °C (final temperature 735 °C) for the two-layer reference model. This illustrates the importance of a sti upper mantle to reach high temperatures in the lower crust (Fleitout & Froidevaux 1980). On the other hand, a single-layer model, with the power-law flow of the upper mantle, shows substantial shear heating at the brittle/ductile transition: at 15 km depth, the temperature increases by 485 °C and reaches 628 °C. Below this transition, the shear-heating e ect decreases sharply, and, below 40 km depth, final temperatures become lower than those of the reference model. The corresponding surface heat flow over the fault is 125 mW m^{-2}.

Variations of the thermal parameters shows that shear heating is much lower in an initially hot lithosphere than in a cold one. This bu ering e ect was expected from previous calculations (Yuen *et al.* 1978; Fleitout & Froidevaux 1980; Brun & Cobbold 1980; Thatcher & England 1998).

3.3 Variations of mechanical parameters

3.3.1 Slip rate

The slip rate on the fault (V) determines the deformation rate, the shear stress profile, and consequently the heat production by shearing. As we assume steady state, our model is appropriate only for faults that maintain a nearly constant slip rate for several million years. As we also assume that the fault separates two blocks of similar thermal state, our model is better adapted for continent/continent transform faults or intracontinental strike-slip faults. Important intracontinental strike-slip faults currently exhibit strike-slip rates of several centimetres per year for several million years (e.g. ≈ 3.5 cm yr^{-1} for the Altyn Tagh fault, Tapponnier *et al.* 1986).

Assuming that 10 cm yr^{-1} is the maximum plausible rate that could be maintained during several million years, we tested rates between 0 and 10 cm yr^{-1}. In this range, the final temperatures significantly increase with the slip rate (Fig. 8a). This increase is not linear and is better fitted by a second-order polynomial: a bu ering e ect induces the final temperatures to saturate at high slip rates (Fig. 8a). However, for common rates, lower than 6 cm yr^{-1}, final temperatures on the fault can be approximately fitted by a linear relationship, the increase of temperature being of the order of 50 °C cm^{-1} yr (Fig. 8a). Slip rate also influences the depth of the brittle/ductile transition: if the slip rate increases, the depth of the brittle/ductile transition decreases following approximately a second-order polynomial (Fig. 8c). Similarly, the surface heat

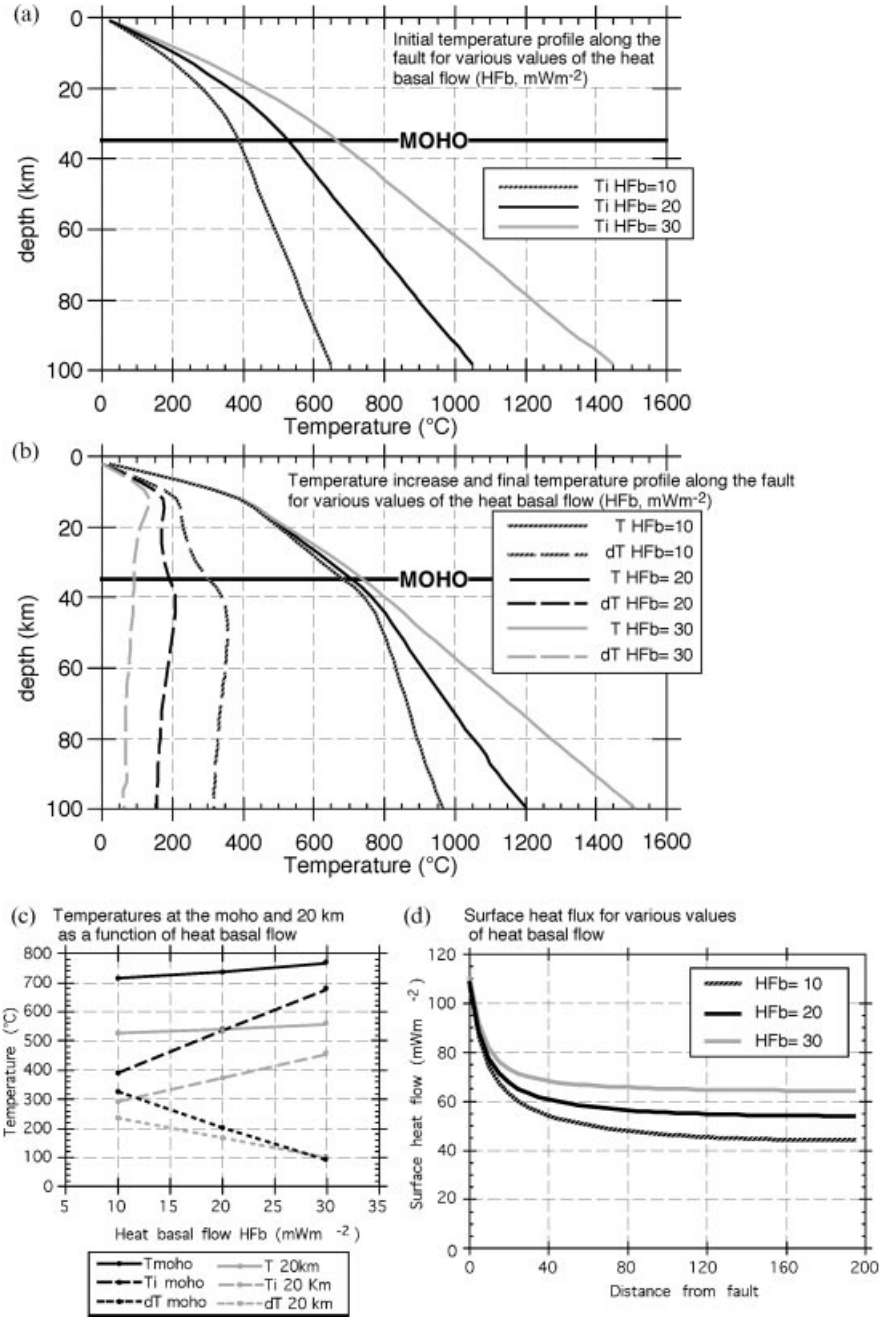

Figure 6. Influence of basal heat flow (HFb) on the thermal structure of lithosphere before and during shearing. All other parameters are set to their reference values (see Table 1). (a) Vertical profile along the fault of initial temperature (Ti) for heat basal flow (HFb) = 10, 20 and 30 mW m^{-2}. (b) Vertical profile along the fault of temperature increase (dT) and final temperature (T) for heat basal flow (HFb) = 10, 20 and 30 mW m^{-2}. (c) Initial temperature, temperature increase, and final temperature on the fault, at the Moho and at 20 km depth, as a function of HFb. (d) Surface heat flow, along a line perpendicular to the fault, for heat basal flow (HFb) = 10, 20 and 30 mW m^{-2}.

flow above the fault increases with the slip rate, following the same type of relationship (Fig. 8d).

3.3.2 *Friction coefficient*

At sample scale, for most crustal rocks, the friction coe cient (F) has a value between 0.85 and 0.6 depending on the level of normal stress (Byerlee 1978). In a large-scale fault zone, however, the e ective friction coe cient probably depends on the level of crushing, lubrication and fluid pressure. Taking Byerlee's value as an upper limit for frictional resistance in a fault zone, we tested values of F between 0.01 and 0.85 (0.6 being the reference value—see Table 1).

The friction coe cient fixes the slope of the brittle part of the strength profile and the associated heat production by shearing. However, as the upper mantle only exhibits brittle deformations for very small friction coe cients ($F \approx 0.1$, Figs 9c and d), final temperatures in the mantle and the lower crust are nearly constant whatever the friction coe cient is (700 ± 25 °C at the Moho, Fig. 9b). The only exception is for

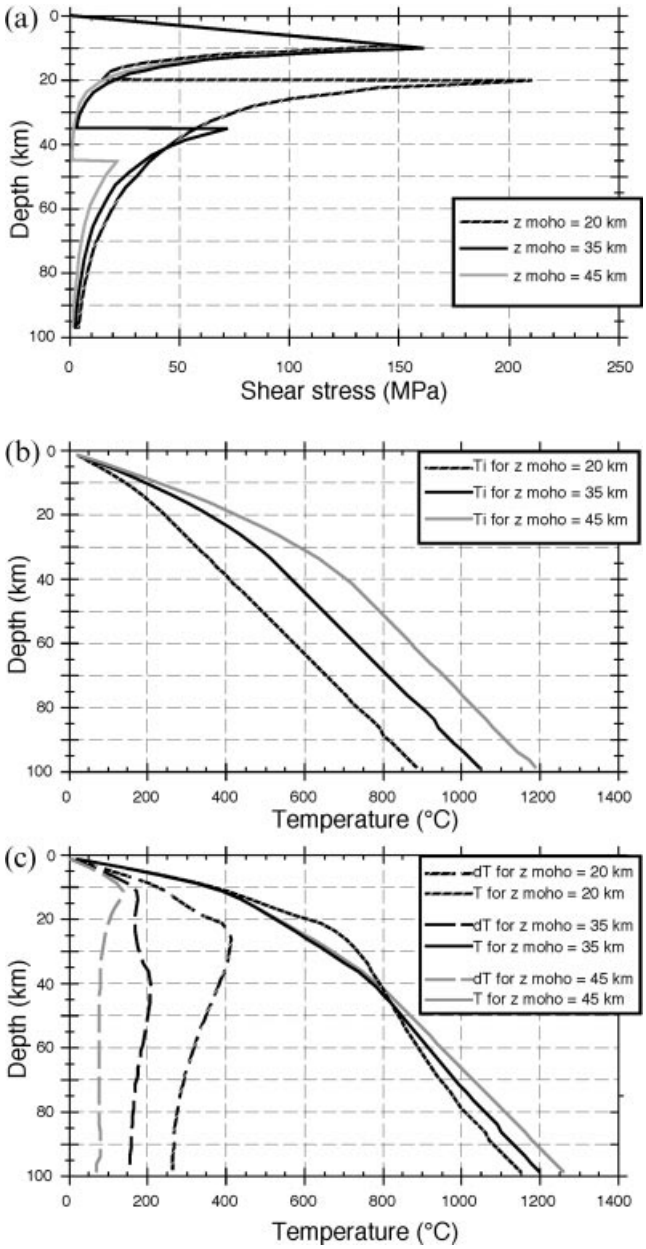

Figure 7. Influence of crustal thickness (M_z) on thermal and mechanical structure of lithosphere before and during shearing. All other parameters are set to their reference values (see Table 1). In all cases, vertical profiles along the fault are shown for $M_z = 20$, 35 and 45 km. (a) Shear-stress profile along the fault. (b) Initial temperature (Ti). (c) Temperature increase (dT) and final temperature (T).

extremely low friction coe cients (e.g. $F = 0.01$), which result in a brittle behaviour of most of the lithosphere, small shear heating and a final temperature at the Moho of only 600 °C (Figs 9a and b). However, such deep brittle deformation, down to 65 km (Figs 9c and d), is incompatible with the fact that seismicity along continental strike-slip faults is restricted in the crust (e.g. Chen & Molnar 1983).

Changes of the friction coe cient have a much greater e ect in the upper crust, significantly changing the final temperatures, the depth of the brittle/ductile transition, and the surface heat flow (Figs 8 and 9). Surface heat flow increases with friction coe cient: for reference parameters it reaches 118 mW m^{-2} for $F = 0.85$ (Fig. 9e). The brittle/ductile transition deepens with decreasing friction coe cient, particularly for values of F below 0.2 (Fig. 9d). Along the San Andreas fault and the Alpine fault in New Zealand, earthquake focal depths extend to 15 and 20 km, respectively (Chen & Molnar 1983). As a first approximation, such depths for the brittle/ductile transition would correspond to low friction coe cients between 0.05 and 0.3 (Figs 8c and 9d) and surface heat flows from 92 to 70 mW m^{-2} (compared with 53 mW m^{-2} before shearing, Fig. 9e). Alternatively, if there is no shear heating along the fault, these depths would correspond to higher friction coe cients ($F > 0.2$), (Fig. 9d) and much higher peak shear stresses (Fig. 2b).

3.3.3 Power-law coefficients

Besides slip rate, ductile shear heating is determined by the power-flow law used. Using a review of power laws of natural rocks (Carter & Tsenn 1987), we tested three of them for each layer (crust and mantle): the hardest, the softest and an intermediate one. Power-flow laws of dry orthopyroxenite (Raleigh et al. 1971), dry Westerly granite (Hansen & Carter 1983) and wet Westerly granite (Hansen & Carter 1983) are used for 'hard', 'average' and 'soft' crust, respectively, while those of dry dunite (Chopra & Paterson 1984), wet Mt Burnet Dunite (Post 1977) and wet Anita bay dunite (Chopra & Paterson 1981) are used for 'hard', 'average' and 'soft' mantle, respectively (Table 1). 'Hard' rheologies induce a much more e cient shear heating, particularly in the middle crust. At 20 km deep, a hard crust is 190 °C hotter than a soft crust (Fig. 10). In the lower crust, hard mantle and soft mantle lead to temperatures at the Moho of 845 °C and 693 °C, respectively (Fig. 10).

3.4 Maximum plausible shear heating along a translithospheric strike-slip fault.

Given the above results, it is possible to determine which parameter values lead to maximum shear heating: a fast slipping fault ($V = 10$ cm yr^{-1}) with a high friction coe cient ($F = 0.6$), a ecting an initially cold lithosphere (HFb = 10 mW m^{-2}, $K = 2.5$ W m^{-1} K^{-1}, radioactive heat production profile 1) composed of hard crust and mantle. A run with these values leads to very high final temperatures of 933 °C at the Moho (temperature increase of 587 °C), and 743 °C at 20 km (temperature increase of 474 °C). This probably corresponds to the absolute maximum shear-heating e ect that one could expect along translithospheric strike-slip faults. This level of shear heating is much higher than expected from previous studies and would eventually induce P–T conditions compatible with partial fusion of granitic rocks at 10 km depth.

4 DISCUSSION: COULD HIGH HEAT FLOW OBSERVED IN LITHOSPHERIC SHEAR ZONES RESULT FROM SHEAR HEATING?

Observations of thermal state along major long-lasting strike-slip faults can be compared with calculations, thus allowing discussion of the basic assumptions of our model.

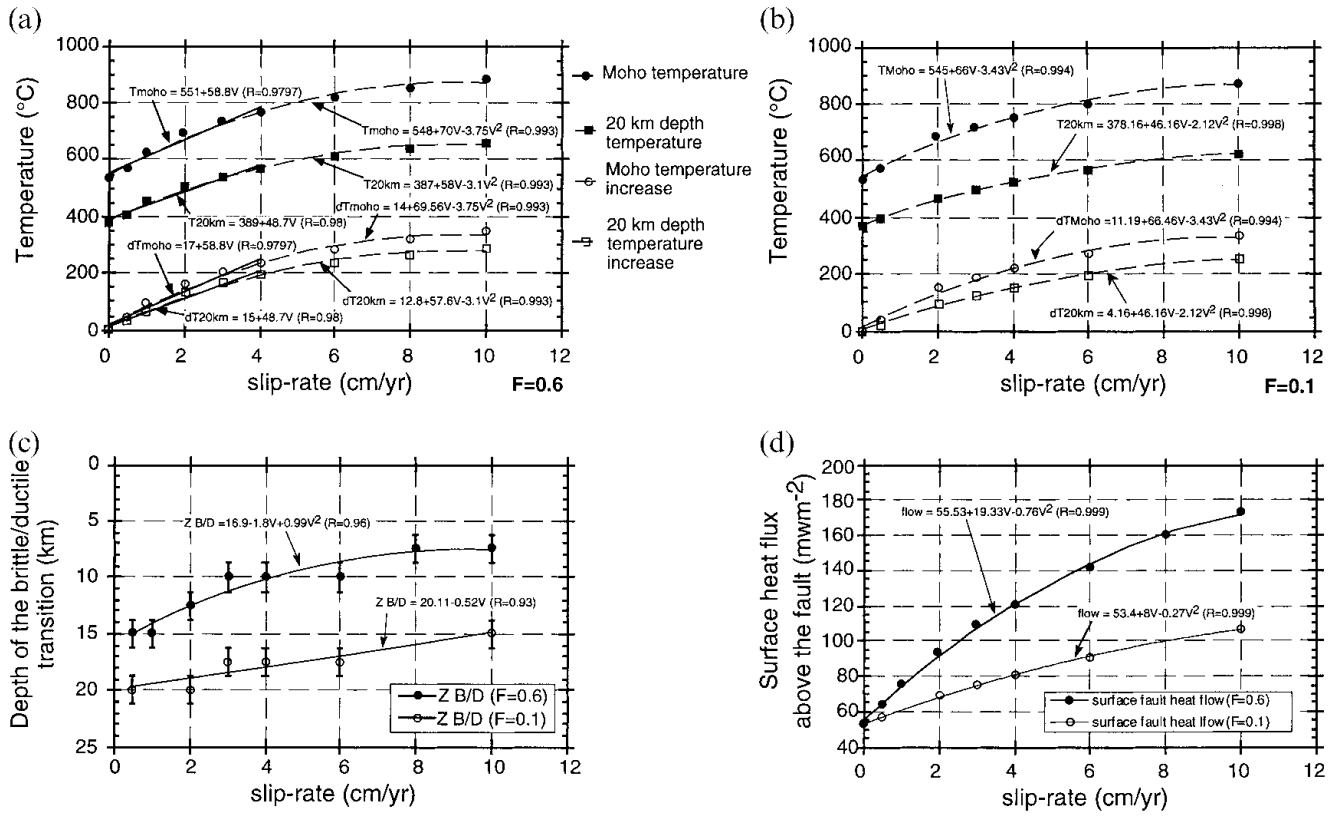

Figure 8. Influence of fault slip rate (V) on the thermal and mechanical state of lithosphere. (a) and (b) Temperature and temperature increase at 20 km depth and 35 km depth (Moho) as a function of slip rate. Dashed lines are fits by a second-order polynomial, straight solid lines are linear fits for slip rates up to 4 cm year^{-1}. In (a) $F = 0.6$ while in (b) $F = 0.1$. All other parameters but slip rate are set to their reference values (see Table 1). (c) Depth of brittle/ductile transition as a function of slip rate for $F = 0.6$ and $F = 0.1$. Solid lines correspond to a second-order polynomial fit to the data. Error bars indicate uncertainty corresponding to the spacing of the calculation grid. (d) Surface heat flow above the fault as a function of slip rate for $F = 0.6$ and $F = 0.1$. Solid lines correspond to a second-order polynomial fit to the data.

Unfortunately, the thermal states of major active strike-slip faults are not well known, the best documented being that of the San Andreas fault zone.

4.1 Thermal state of the active North America/Pacific transform boundary

The absence of a localized heat-flow anomaly associated with the present-day San Andreas fault trace (Lachenbruch & Sass 1980) has been taken as evidence for low shear stress and/or the absence of shear heating along major strike-slip faults. However, the San Andreas fault zone has a complex history, which should be taken into account. Since the onset of the subduction of the Farallon–Pacific ridge below North America, at approximately 30 Ma, the transform boundary between North America and the Pacific has been a lengthening right-lateral fault zone linking two triple junctions that migrate in opposite directions (Atwater & Molnar 1973). Within this broad zone, the main fault has jumped eastwards several times (e.g. Dickinson 1981) and coincides with the San Andreas fault only since 7.5–5 Ma (Dickinson & Snyder 1979). Thus, the thermal state of the San Andreas zone probably results from various processes: subduction, opening of an asthenospheric window, and progressive eastward migration of the strike–slip boundary.

In the area south of $\approx$35°N, below which the Farallon–Pacific ridge subducted, the present-day transform motion takes place in a broad zone with several surface strike-slip fault strands, and with no heat-flow anomaly (Fig. 19 of Lachenbruch & Sass 1980). North of 35°N, where deformation is localized along one main fault strand, there is a large-scale, $\approx$80 km wide, heat-flow anomaly—the Coast Ranges anomaly (Lachenbruch & Sass 1980) (Fig. 11a). In this area, heat flows are between 50 and 100 mW m^{-2} near the fault, and drop to 42–55 mW m^{-2} 80 km farther east. Along strike, the Coast Ranges heat-flow anomaly decreases towards the north and finally vanishes at the Mendocino triple junction (Fig. 12 of Lachenbruch & Sass 1980). The heat-flow anomaly is thus clearly associated with the fault zone.

Some authors have attempted to explain this anomaly by the e ect of the northward migration of the Mendocino triple junction, without a contribution from shear heating (e.g. Dickinson 1981; Zandt & Furlong 1982). In this case, a good fit to the observed anomaly is only obtained for extreme conditions, such as the opening of a lithospheric gap and upwelling of the asthenosphere along the triple-junction path (e.g. Lachenbruch & Sass 1980). On the other hand, shear-heating models have been proposed for the San Andreas fault, and seem to explain the main heat-flow characteristics satisfactorily. Using a previous version of the model presented in this paper, Ricard *et al.* (1983) obtain a better fit of the along-strike shape of the heat-flow anomaly than if shear heating is neglected, but with a modelled across-strike anomaly narrower than observed. Thatcher & England (1998) also

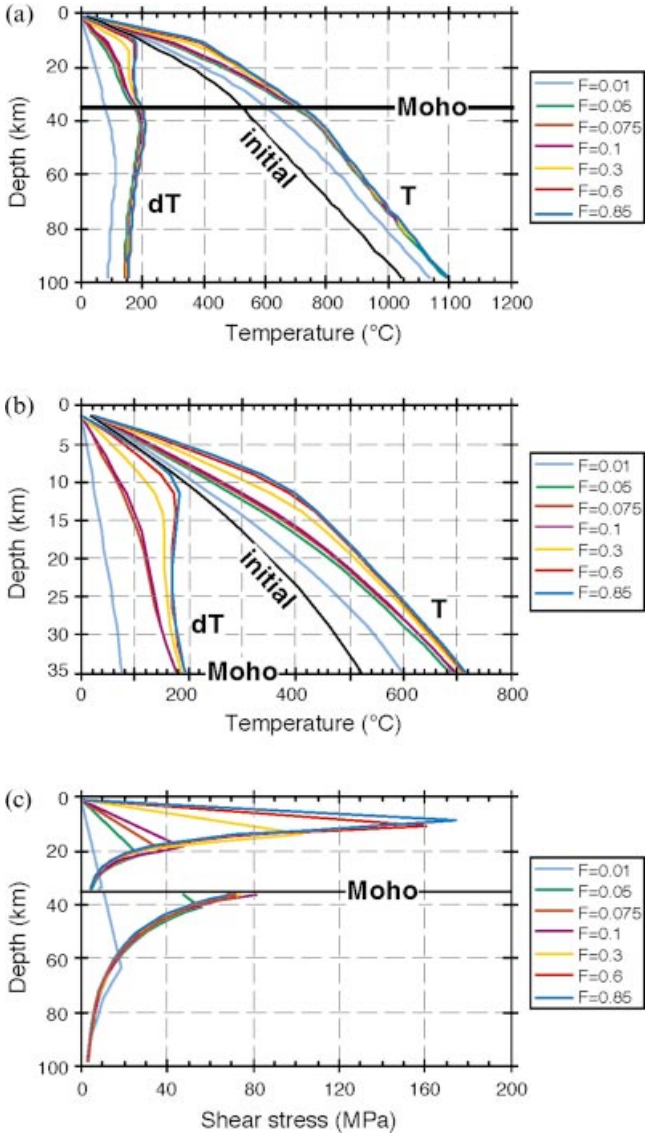

Figure 9. Influence of the friction coe cient on lithospheric thermo-mechanical structure during shearing. The friction coe cient is the same in the crust and upper mantle. All other parameters are fixed to their reference value (see Table 1). (a) Lithospheric vertical profile along the fault of final temperature (T) and temperature increase (dT) for friction coe cients between 0.01 and 0.85. (b) Crustal vertical profile along the fault of final temperature (T) and temperature increase (dT) for friction coe cients between 0.01 and 0.85. (c) Lithospheric strength profile for friction coe cients between 0.01 and 0.85. (d) Depth of brittle/ductile transition as a function of friction coe cient. Reported depths correspond to the base of the deeper brittle element. Box heights indicate uncertainty corresponding to the spacing of the calculation grid. Dark and light shading represents runs with and without shear heating, respectively. Note that brittle deformation occurs in the upper mantle only for very small friction coe cients. (e) Surface heat flow, above the fault, as a function of friction coe cient.

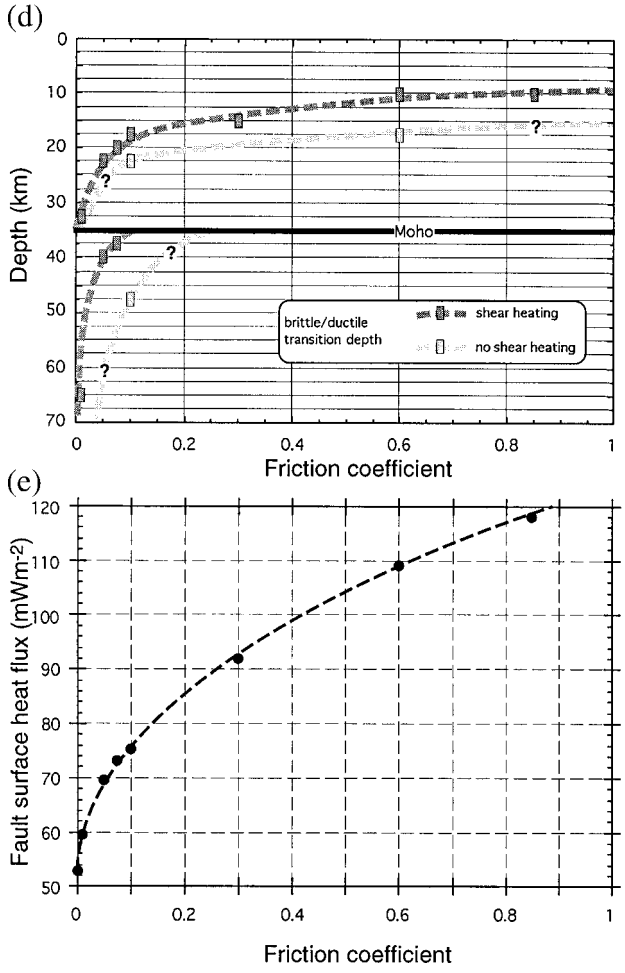

Figure 9. (*Continued.*)

estimated that ductile shear heating in the lower crust or in the upper mantle might explain the heat-flow amplitude, and that shear heating on minor faults could broaden the anomaly. In their model, shear-heating intensity depends weakly on slip rate, implying that even minor faults may induce strong heat production. Note, however, that this weak dependence of shear heating on slip rate rests upon their choice of an over-simplified Newtonian rheology for earth materials, in contradiction with most experimental results.

The total displacement of Tertiary markers on the presently active fault strand is close to 300 km (Irwin 1990), mostly accumulated since 7.5 Ma (Dickinson & Snyder 1979). This implies an average rate of ≈ 4 cm yr^{-1}, close to the rate of ≈ 3.5 cm yr^{-1} deduced from o set Holocene markers (Sieh & Jahns 1984). A run of our model assuming a crustal thickness of 25 km (Gary & Mooney 1990), a radioactivity decreasing with depth, and a basal heat flow of 20 mW m^{-2} leads to a surface heat flow before shearing of 48 mW m^{-2}, compatible with what is observed out of the fault zone (35–55 mW m^{-2}, Fig. 11a). After shearing at a rate of 4 cm yr^{-1}, using the reference rheologies and a low friction coe cient ($F = 0.2$), the surface heat flow above the fault rises to 87 mW m^{-2}, thus approaching the intensity of the Coast Ranges heat-flow anomaly (Fig. 11a). Along the San Andreas fault the base of the seismogenic layer is 10–15 km deep (Sibson 1984). This imposes the condition that F be smaller than 0.3. A friction coe cient smaller than 0.15 would lead to a brittle upper mantle, which is not indicated by seismicity. If F is the same in the crust and in the mantle, it is therefore constrained to be between 0.15 and 0.3. Such a small e ective friction coe cient is in accord with the observation of principal horizontal compressive stresses being almost perpendicular

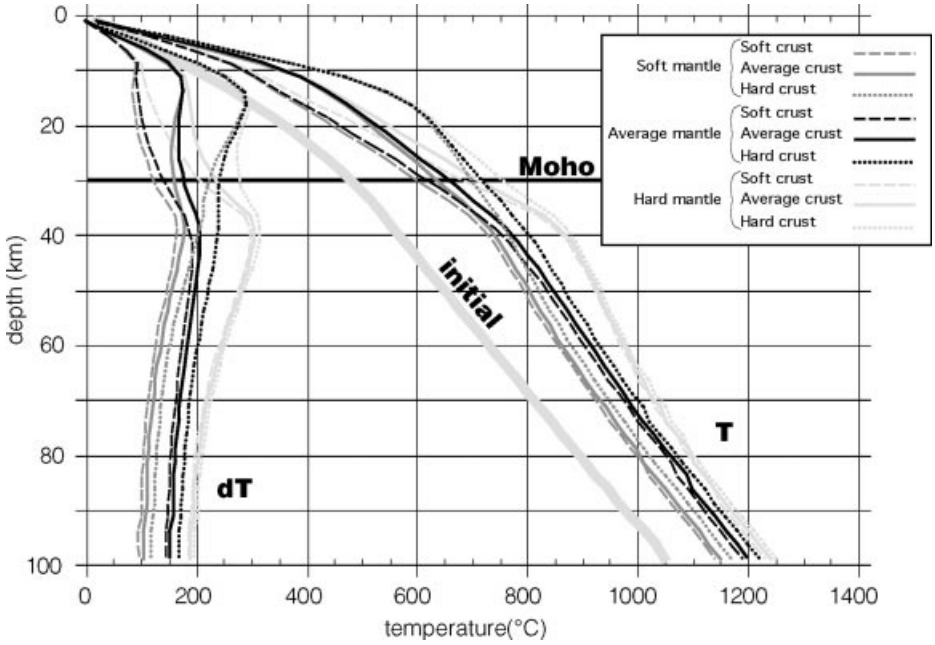

Figure 10. Influence of possible flow laws on lithospheric temperature structure along the fault during shearing. Hard, average and soft crust and mantle refer to various power-flow laws used: see text and Table 1 for details. Initial: geotherm before shearing; dT: temperature increase due to shear heating; T: final temperature.

to the fault zone (Zoback *et al.* 1987; Mount & Suppe 1987). For a friction coe cient of 0.2, maximum shear stresses in the crust are $\approx$70 MPa (Fig. 11c). This corresponds to a 4.7 MPa km^{-1} vertical shear-stress gradient to compare with the $\approx$7.9 MPa km^{-1} measured near the San Andreas fault in wells up to 850 m deep (Mc Garr *et al.* 1982). In the absence of shear heating, our calculations indicate a brittle upper mantle and a deep ($\geq$20 km) crustal brittle/ductile transition, even for very high friction coe cients ($>$0.6) that would correspond to high crustal shear stresses ($>$325 MPa).

However, notwithstanding that we take into account shear heating in the whole lithosphere, the modelled surface heat-flow anomaly vanishes less than 50 km from the fault (Fig. 11a). This is a much smaller distance than that observed (Lachenbruch & Sass 1980). The broad measured anomaly has been interpreted as due to shear heating either on horizontal planes (Lachenbruch & Sass 1980) or in a 80 km wide shear zone (England & Molnar 1991). Given the complex history of the fault zone both hypotheses are plausible although clearly *ad hoc*. The existence of a wide shear zone is in contradiction with the fact that shear heating necessarily induces a progressive strain localization. It is possible that steady state is not yet reached in California and that the upper mantle still deforms over a wide zone. Alternatively, in our steady-state model, temperature increase in the lower crust and upper mantle occurs in a wide zone. For example, at a depth of 20 km, the temperature increases by 150 °C 25 km away from the fault (Fig. 11b). From such depths, hot fluids could migrate upwards, thus increasing and widening the surface heat-flow anomaly. In the upper crust, fluids could also migrate laterally along pre-existing discontinuities (faults, bedding, etc.), broadening the anomaly further. Supporting this idea, intense fluid migration in the upper crust has been suggested west of the fault on the basis of high H_2O content, high $\delta^{18}O$, and low δD of granitoids (O'Neil & Hanks 1980). Such measurements are unfortunately not available east of the fault, where the coast range anomaly is better defined. However, the lack of hot springs east of the San Andreas fault seems to limit the importance of such phenomena, unless heat discharge occurs in numerous springs at temperatures only slightly above the ambient. Obviously, heat-flow measurements do not provide enough constraints on the deep thermal structure of the fault zone to distinguish between these hypotheses. In any case, our model underestimates the thermal-anomaly width and thus probably the total heat production.

4.2 High-temperature metamorphism in exhumed strike-slip shear zones

Large, exhumed strike-slip shear zones are listed in Table 2 with their main thermal characteristics. These shear zones share two common features. First, down to the base of the crust (granulite facies), strike-slip deformation appears to be localized in mylonitic zones usually less than 25 km wide. Second, metamorphic peak temperatures are high in the fault zones, and often lead to crustal partial melting.

We distinguish two main types of strike-slip faults: orogen-parallel and orogen-oblique. Orogen-parallel strike-slip faults that develop in the hanging walls of subduction zones (e.g. the Sumatra fault, Fitch 1972), and in internal part of orogenic zones (e.g. the Insubric fault in the Alps, Lacassin 1989) result from slip partitioning between thrusting and strike-slip faulting. Together with shear heating, subduction and/or thickening processes a ect the thermal regime of such faults. This must be kept in mind during any comparison with geological data. On the other hand, orogen-oblique strike-slip faults develop in most cases during indentation tectonics (e.g. Tapponnier & Molnar 1976) and cut across contemporaneous thrusts and fold. The Altyn Tagh Fault of northern Tibet (e.g. Peltzer *et al.* 1988) is a good example of a present-day cross-cutting

Table 2. Thermal regime in some strike-slip fault zones.

Name	**location**	**type**	**length** (L in km) **width** (w in km) **offset** (o in km) **shear sense** (S)	**timing** (T) **strike-slip rate** (r in cm/yr)	**Metamorphism** P–T estimates	**synkinematic magmatism** $^{87/86}$Sr of granitoids	**References**
Alpine fault	– New Zealand South Island – Transform between Pacific & Australia	Plate boundary • orogen oblique in the Miocene • orogen-parallel since 10–5 Ma	L ≈ 600 km inland w 1.5 km o ≈ 480 km S: dextral	T: since ≈ 36 Ma r ≈ 1–2.5 in the Miocene, ≈ 3.5 with compression since.	Low amphibolite T: 490–540 °C P: 5.4–6.6 kb? Argon and Sr Depletion	some pegmatitic dykes?	Sibson *et al.* (1979) Grapes (1995) Scholz *et al.* (1979)
Great Slave Lake shear-zone **GSL sz**	– North West Territories Canada – Boundary between the slave and Churchill provinces	Intracontinental orogen-oblique	L ≈ 1300 km w ≤ 25 km o ≈ 300–700 km S: dextral	T ≈ 2–1.9 Ga	Granulite to greenshist belt 1: 840 °C & 8.2 kb belt 2: 880 °C & 7.5 kb belt 3: 680 °C & 4 kb	synkinematic batholithe (γ and Kf-γdiorite) and migmatites. some late diabase dikes.	Ho man (1987) Hanmer (1988)
Ailao Shan–Red River **ASRR sz**	– SE Asia – Boundary between Indochina and South China.	Intracontinental orogen-oblique	L ≥ 1000 km inland w ≈ 20 km o ≥ 700 ± 200 km S: sinistral	T: Oligo-Miocene, from ≈40? to 16 Ma r ≈ 4 ± 1	Amphibolite (P5kb-T700 °C) to greenshist	synkinematic leucoγ layers and monzonitic bodies (0.7071 to 0.7234)	Leloup *et al.* (1995) Schärer *et al.* (1994) Zhang (1995)
Dom Feliciano belt (Brazil)	– Southern Brazil–Uruguay – internal part of collision belt between Rio de la plata & Kalahari cratons	Orogen-parallel	L > 500 km w ≤ 15 km S: sinistral	T: Pan African	prograde metamorphism from ≈550 °C to ≈675 °C ≈425 °C at ≈3 Kb	2 generations: 1) γdiorite-adamelites (0.7163) 2) Sodi potassic to peralcaline leucoγ (0.7329)	Tommasi *et al.* (1994)
South American shear-zone **SA sz**	– South Brittany (France) – Separate central and Southern american domain	Orogen-parallel	L > 300 km w: 2 branches hundreds m wide separated by a deformed belt up to 60 km wide. S: Dextral	T: Carboniferous ?–330–290? Ma	triple point And-Sill-Ky (≈T 450 °C, P 4.5 kb) to greenschist	Numerous and large 2 micas leucoγ resulting from anatexis of the sediments. 0.703 to 0.7102 (increase with time)	Jegouzo (1980) Strong & Hanmer (1981)
Coïmbra–Badajoz–Cordoba shear-zone	– Central Portugal & Spain	Orogen-parallel	L > 400 km w ≈ 20 km S: sinistral	T: Upper Carboniferous	granulite?–amphibolite–greenshist	Numerous and large 2 micas leucogranites	Burg *et al.* (1981)
Serra da Freita shear-zone	– Central Portugal	Orogen-parallel	L > 70 km w ≈ 2 km S: sinistral	T: Carboniferous	amphibolite (sillimanite)	Large 2 micras leucogranite 0.7136	Reavy *et al.* (1991)

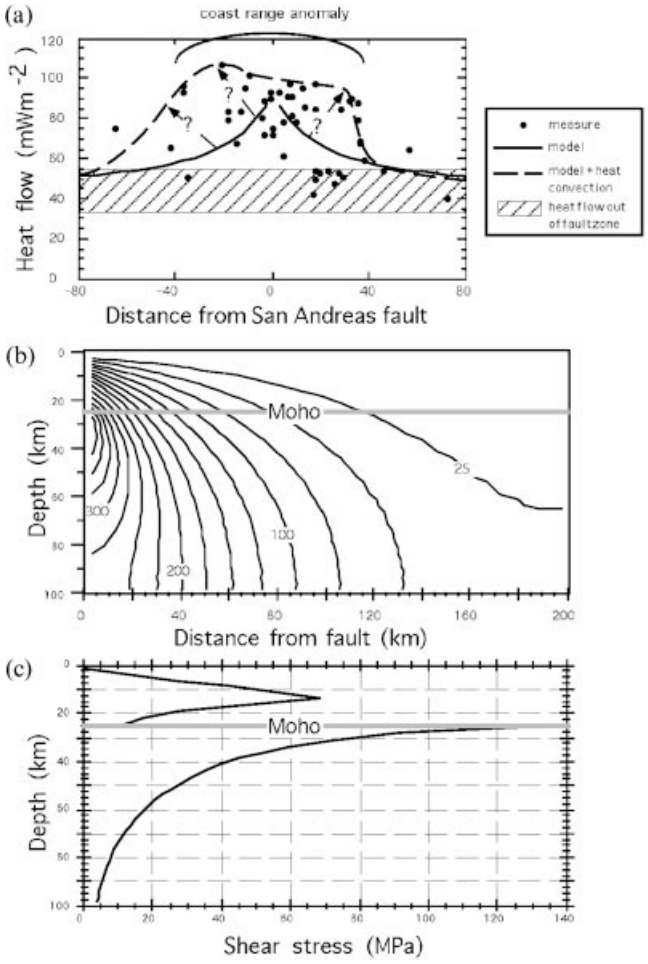

Figure 11. Shear-heating model applied to the San Andreas fault between 35 and 40°N. Run executed with the following parameters: $K = 2.5\ W m^{-1} K^{-1}$, $HFb = 20\ mW\ m^{-2}$, Q_r (in $mW\ m^{-3}$) = 2 from 0 to 7.5 km, 1.6 to 15 km, 0.4 to Moho, $M_z = 25$ km, $V = 4\ cm\ yr^{-1}$, Fc = 0.1, Fm = 0.1, average crust, average mantle. (a) Heat-flow measurements (regions 3, 4, 5 and 6 of Lachenbruch & Sass 1980) plotted together with heat flow from model (continuous line) and an estimate of heat flow considering substantial heat advection in the middle and upper crust (dashed line). The diagonal pattern shows the heat-flow value outside the San Andreas fault zone. (b) Temperature increase in the lithosphere due to shear heating according to the model (no heat advection). In the crust, a temperature increase of more than 100 °C is restricted to within 50 km of the fault. (c) Corresponding lithospheric shear-stress profile in the fault zone.

strike-slip fault. Far from the collision front, such faults a ect a mildly deformed lithosphere, and their characters may be directly compared with the results of our model.

4.2.1 *Shear heating in orogen-oblique strike-slip shear zones*

The Alpine fault of New Zealand: The New Zealand Alpine fault, part of the Australia–Pacific plate boundary, is a ≈600 km long straight fault marked by a ≈1.5 km wide stripe of cataclasites, pseudotachylites and mylonites (Sibson *et al.* 1979). The fault cuts and o sets by 480 km a Jurassic-Cretaceous subduction complex (Wellman 1955). Most of this o set took place in the Oligo-Miocene (e.g. Cooper *et al.* 1987), when the Australia/Pacific motion was almost purely strike slip, with a rate of 1–2.5 cm yr^{-1} (e.g. Stock & Molnar 1987).

Close to the fault, the Mesozoic schistosity is transposed by a steeper one, parallel to the fault (e.g. Findlay 1987). This transposition corresponds to the formation of metamorphic isograde parallel to the Alpine fault: metamorphism increases from phrenite-pumpellyite ≈14 km from the fault (≈260 °C and 4.2 kb) to garnet-oligoclase amphibolite facies within 6 km (e.g. Grapes 1995). Along the fault, in the K-feldspar zone, pressure–temperature conditions of metamorphism are in the range 5.4–6.6 Kb (20–24 km) and 490–540 °C (Grapes 1995). K–Ar ages, which are Cretaceous (150–120 Ma) more than 25 km east of the fault (e.g. Harper & Landis 1967), show a progressive younging towards the fault, and become younger than 30 Ma less than 10 km from it (e.g. Adams & Gabites 1985; Sheppard *et al.* 1975). Fission-track ages follow the same trend, with no apatite age older than 35 Ma less than 40 km from the Alpine fault and no zircon age older than 10 Ma in the amphibolite zone (Kamp *et al.* 1989).

It is thus clear that, during the Cenozoic, the low-grade schists metamorphosed in the Mesozoic su ered a second prograde metamorphism coeval with strike-slip deformation along the Alpine fault. Shear heating is a very appealing mechanism to explain such a thermal event. Scholz *et al.* (1979) calculated that, if depth-averaged shear stress on the fault was in excess of 50 MPa, the temperature increase induced by shear heating could lead to argon degassing, explaining the observed age pattern. Our model confirms this calculation. The present-day crustal thickness far from the Alpine fault (≈30 km; Woodward 1979) gives a lower bound for the crustal thickness in the Oligocene. At this time, the geotherm was thus probably close to our initial geotherm calculated for a crustal thickness of 35 km (Fig. 12). After strike-slip faulting at a rate of 2.5 cm yr^{-1}, and for the reference parameters, our model indicates that temperatures close to 540 °C are attained in the shear zone at a depth of ≈23 km, in very good agreement with the *P–T* estimates. This would imply at least ≈23 km of late Cenozoic uplift east of the Alpine fault at an average rate of ≈2.3 mm yr^{-1} in order to bring these high-temperature rocks to the surface. Such rates are compatible with the uplift rates of 2.6–7 mm yr^{-1} estimated for the last ≈340 000 years (Bull & Cooper 1986). Indeed, since ≈10 Ma, the relative Australia/Pacific motion has been oblique to the Alpine fault (e.g. De Mets *et al.* 1990; Berryman *et al.* 1992; Wellman 1984), thus inducing rapid uplift of the Southern Alps that fringe the fault to the SE. Such uplift has deformed the metamorphic isograde formed previously during purely strike-slip deformation. Several authors thus explain the increase of metamorphism towards the fault by an increase of exhumation rather than shear heating (e.g. Wellman 1979; Adams 1979). This hypothesis seems unconvincing because it needs an unlikely '^{40}Ar partial retention zone' to explain the age pattern (e.g. Adams & Gabites 1985; Kamp *et al.* 1989), and does not fit with the thermobarometric data nor the present-day topography. Nonetheless, only further field work could confirm shear heating as the primary metamorphic process.

Great Slave shear zone (NW territories, Canada): Deep strike-slip mylonites crop out in the ≈1300 km long Precambrian Great Slave Lake (GSL) shear zone of NW Canada (Table 2) (e.g. Ho man 1987; Hanmer 1988). At large scales, the fault zone cuts across previous structures and o sets the Thelon and Taltson volcanic arcs. Finite dextral o set is estimated to

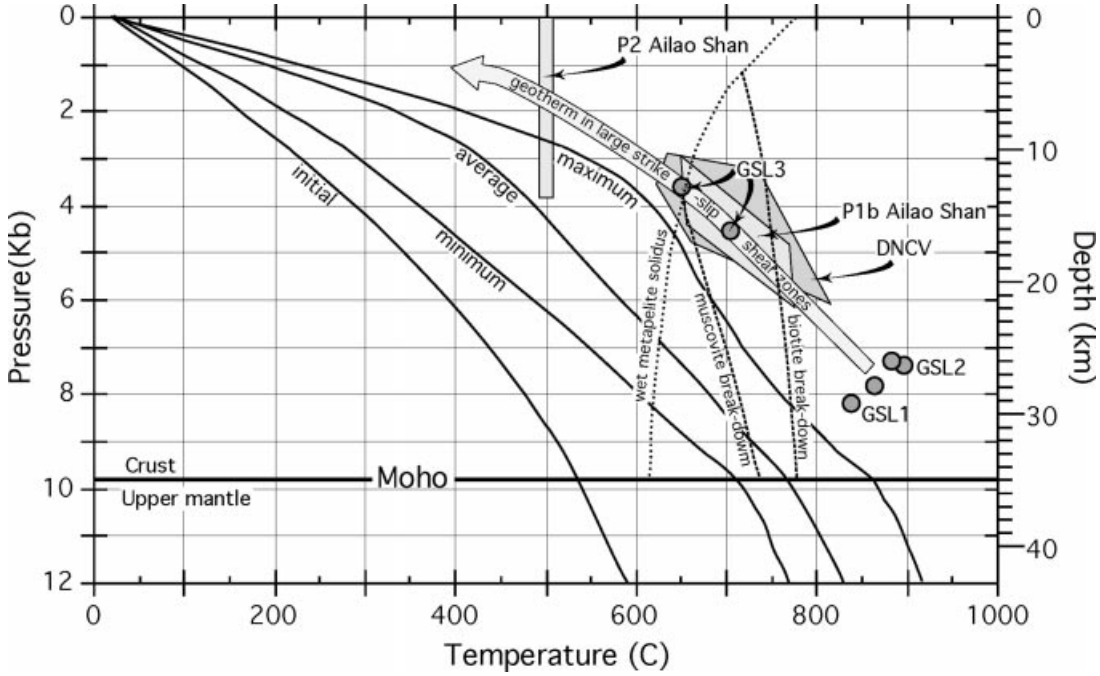

Figure 12. Shear-zone crustal geotherms calculated for a 4 cm yr^{-1} shear rate compared with thermobarometric data of ASSR and GSL shear zones and crustal melting curves. *Steady-state model geotherms.* Initial: reference model before shearing; Average: $V = 4$ cm yr^{-1}, otherwise reference parameters; maximum: maximum shear heating for $V = 4$ cm yr^{-1} ($F = 0.6$, hard crust, hard mantle); Minimum: minimum shear heating for $V = 4$ cm yr^{-1} ($F = 0.1$, soft crust, soft mantle). *Simplified crustal melting curves.* Wet solidus: H_20-saturated metapelite solidus (Thompson 1982); Muscovite breakdown: muscovite dehydration melting (Mus + Alb + Q → Ksp + Als + L) (Petö 1976); Biotite break-down: biotite dehydration melting (Bio + Als + Pl + Q → Gar + Ksp + L) (Le Breton & Thompson 1988). *P–T estimates.* ASRR shear zone: Peak (P1b and DNCV) and retrograde (P2) paragenesis (Leloup & Kienast 1993; Leloup, unpublished data); Great slave lake shear zone (GSL): GSL1, 2 and 3 correspond to *P–T* estimates in the granulite, upper amphibolite and amphibolite belts of the shear zone, respectively (Hanmer 1988).

be between 300 and 700 km. The shear zone, up to 25 km wide, is made of five parallel mylonitic belts (1–5) formed under granulite to greenschist metamorphic facies. Through time, deformation progressively occurred in narrower belts of lower metamorphic grade (Hanmer 1988). Belts 1 and 2, of granulite and upper amphibolite facies, respectively, formed in lower crustal conditions at high temperatures (≈8.2 Kb and ≈840 °C for belt 1, and ≈7.5 Kb and ≈880 °C for belt 2) (Fig. 12). Belt 3 formed at around 15 km depth (≈4 Kb) at temperatures of about 680 °C (Fig. 12). Belts 4 and 5 are 1–1.5 km wide zones of rocks deformed under greenschist facies in which *P–T* conditions are di cult to assess. During strike-slip faulting, the shear zone has been progressively uplifted and cooled along a steep geothermal gradient. Strike-slip deformation was coeval with extensive *in situ* melt production, as attested by syntectonic migmatization in belts 1 and 2, and syntectonic granitoid intrusions in belts 1–4. Some late-syntectonic mafic dykes (diabase) are found in belt 2. U/Pb ages of zircons from the intrusions bracket deformation age between ≈1.98 and ≈1.925 Ga (Hanmer 1988).

Strike-slip deformation along the GSL occurred at high temperatures in a narrow zone. This suggests that shear heating was the main mechanism of producing heat along this fault. To obtain a final geotherm compatible with the *P–T* estimates in the GSL, it is necessary to use parameters leading to the absolute maximum shear-heating e ect that one could expect along a translithospheric strike-slip fault ($V = 10$ cm yr^{-1}, $F = 0.6$, hard crust and mantle, see Section 3.4). While very unlikely, such a possibility cannot be ruled out, as the old age of the GSL precludes any determination of the palaeo-slip rate.

Ailao Shan–Red River shear zone (China and Vietnam): The Ailao Shan–Red River (ASRR) shear zone is possibly the best-documented example of a mid-crustal orogen-oblique shear zone. This zone allowed the lateral escape of the Indochina block in response to the India/Eurasia collision (e.g. Tapponnier *et al.* 1986; Tapponnier *et al.* 1990; Leloup *et al.* 1995). The ASRR shear zone is nearly 1000 km long with ductile left-lateral strike-slip shear exposed in four elongated mylonitic cores less than 20 km wide. Displacement is estimated at 700 ± 200 km (Leloup *et al.* 1995). Thermo-barometric studies show that transcurrent strain occurred under amphibolite facies conditions (3–8 kb and 550–825 °C; Fig. 12). Leucocratic and monzonitic melts were emplaced during strike-slip shear. Such rocks yield U/Pb ages between 26.3 and 22.4 Ma, implying Lower Miocene shear (Schärer *et al.* 1990; Schärer *et al.* 1994; Zhang 1995). Geochemical data indicate that magmatic rocks in the ASRR zone originated from partial melting in both the lower and middle crust (Zhang 1995). A strike-slip rate of 4 ± 1 cm yr^{-1} seems to have been maintained between ≈35 and 16 Ma (Briais *et al.* 1993; Leloup *et al.* 1994; Harrison *et al.* 1996). The crust is ≈35 km thick (Yan Qizhong *et al.* 1985) and Tertiary thickening is moderate along most of the fault. This led Leloup & Kienast (1993) to propose shear heating as the main cause of the high temperatures observed in the ASRR shear zone.

The geotherm calculated for reference parameters (crust 35 km thick, HFb = 20 mW m^{-2}) and a strike-slip rate of 4 cm yr^{-1} (labelled 'average' on Fig. 12) is much hotter than the initial one but still too cold to explain the ASRR peak metamorphic conditions. The maximum shear-heating e ect would be obtained using a high friction coe cient (i.e. $F = 0.6$)

and hard rheologies. The resulting geotherm (labelled 'maximum' on Fig. 12) is barely compatible even with the higher P and lower T estimates in the ASRR shear zone.

P–T conditions recorded in the ASRR and GSL shear zones are similar and define a geotherm probably typical of large continental orogen-oblique shear zones (Fig. 12). In both cases, our calculations fail to model this geotherm, or do it for unrealistic parameters only (e.g. slip rate of 10 cm yr^{-1} for the GSL). Surprisingly, our model thus underestimates the final temperatures. This was not expected, as several characteristics of the model tend to maximize the shear-heating e ect: (1) 100 per cent of the mechanical energy is converted to heat; (2) latent-heat-consuming metamorphic reactions are neglected; (3) steady state is assumed, requiring several million years of uninterrupted strike-slip faulting; (4) shear heating is taking place in both ductile and brittle fields of the crust and mantle.

Our choice of using a simplified solution, neglecting shear heating on horizontal planes, leads to a slight underestimation of the shear heating e ect (see Appendix A). This underestimation is, however, too small to explain the discrepancy between the model results and the observed P–T conditions. In our model, heat transfer occurs only by conduction, while in nature heat advection processes may be important. Advection might transport heat from regions where it is produced, mostly at the brittle/ductile transition and in the upper mantle, towards colder areas. Furthermore, in a long-lasting shear zone, such a mechanism may increase the global heat production. Indeed, if heat di uses slowly, temperatures rise rapidly near the heat source, bu ering heat production by shear heating. On the other hand, if heat is removed from where it is produced, the bu ering e ect is reduced as sheared rocks remain colder and thus sti er.

4.2.2 *Heat advection in strike-slip shear zones*

Various mechanisms may account for a more e cient heat transport than the isotropic di usion considered in our model. In shear zones, the mylonitic schistosities and foliations are parallel to the zone. Sedimentary rocks show a strong anisotropy in thermal conductivity, which is low (<2 W m^{-1} K^{-1}) perpendicular to bedding and up to three times higher parallel to it (Deming 1994). If such anisotropy existed in foliated metamorphic rocks, heat would di use more rapidly along the shear zone than across it, even in the case of purely conductive heat transfer. Furthermore, hot fluids move easily along the mylonitic fabric, making the shear zone a good heat pathway. Melted rocks and rising magmas can be very e cient heat carriers. In dikes feeding some Himalayan leucogranite batholiths the estimated magma ascent rates of melts produced by muscovite breakdown are of the order of 1 m s^{-1} (Scaillet *et al.* 1996). This mechanism could thus carry heat nine orders of magnitude more e ciently than conduction. Melt ascent is very probably enhanced in a vertical shear zone. However, is shear heating able to produce crustal partial melting?

In most cases, modelled final temperatures in the lower crust are hotter than the water-saturated solidus for metapelites (Fig. 12). Nevertheless, substantial melting in such conditions would require a large reservoir of free water and a large porosity, both unexpected in the lower crust. In the absence of free water, partial fusion may occur by dehydration melting (or breakdown) of hydrous minerals (mainly micas and amphiboles) (e.g. Thompson & Conolly 1995; Gardien *et al.* 1994). According to Thompson & Conolly (1995), a dry rock composed of a fertile 'granite minimum' component (40 wt per cent) and a refractory component, located at 30 km depth, produces $\approx$5.5 vol per cent of melt when the temperature of muscovite breakdown is reached ($\approx$700 °C). The melt fraction attains $\approx$8 vol per cent just below the temperature of biotite breakdown ($\approx$770 °C) and suddenly rises to $\approx$16 vol per cent above it (Fig. 2 of Thompson & Conolly 1995). In the case of the ASRR shear zone ($V = 4$ cm yr^{-1}), conditions compatible with partial melting are easily reached (Fig. 12). The modelled geotherms are compatible with water-saturated partial melting below $\approx$30 km for soft rheologies and low friction coe cient ('minimum', Fig. 12), $\approx$25 km for reference parameters ('average') and $\approx$16 km for hard rheologies and high friction ('maximum'). Muscovite breakdown would occur below $\approx$32 km ('average') or 21 km ('maximum'), while biotite breakdown would occur only for maximum conditions below $\approx$32 km.

Comparing the modelled geotherms with the peridotite solidus permits the discussion of the possibility of mantle partial melting (Fig. 13). For a dry upper mantle, temperatures before and during shearing are far too low to produce partial melting of the lithospheric mantle. Even decompression by a dramatic vertical uplift (arrow 1 on Fig. 13) could not induce such melting. For an improbable water-saturated upper mantle, partial melting may be reached at much lower temperatures (Fig. 13). It would occur at the base of the lithosphere before shearing (100 km depth) and below $\approx$76 km (23 kb) to $\approx$57 km (17 kb) during shearing, depending on the final geotherm considered (Fig. 13). As the upper mantle probably contains a small fluid fraction, an intermediate solidus should be used. In that case, partial melting could occur during shearing in the lower part of the lithosphere, below $\approx$86 km (26 kb) (Fig. 13). After shearing, decompression melting of the lithospheric mantle would be possible for rocks initially located in the lower part of the lithosphere (arrow 2 on Fig. 13), but in most cases after a large adiabatic uplift (arrow 3 on Fig. 13). Large rapid uplift is unlikely to occur along the entire length of a strike-slip shear zone but may exist locally, for example below large pull-apart basins. The contribution of mantle-derived melts could be at the origin of the mafic dykes observed in the GSL shear zone and could have enhanced lower crustal melting and alkaline magma production in the ASRR shear zone. In most strike-slip zones, however, the mantle contribution to magmatism seems limited and most plutonic rocks show $^{87/86}$Sr ratios greater than 0.7 (Table 2).

Lithospheric-scale shear heating and heat advection by rising melts or fluids is thus a plausible mechanism to explain high-grade metamorphism and high heat flows in large orogen-oblique strike-slip shear zones. We propose a model of a lithospheric shear zone (Fig. 14) where high temperatures in the lower crust are triggered by shear heating in the upper mantle. Melt ascent in the shear zone accentuates the thermal anomaly associated with the fault and may promote strain localization. Mantle melting at the base of the lithosphere, by shear heating and eventually with local decompression, may further enhance crustal melting.

4.2.3 *Shear heating in orogen-parallel strike-slip shear zones*

Most strike-slip shear zones that have developed within orogenic belts show a spatial and temporal coincidence of transcurrent shear, high-temperature metamorphism and granitoid magmatism (e.g. Hutton & Reavy 1992). For example, the Hercynian

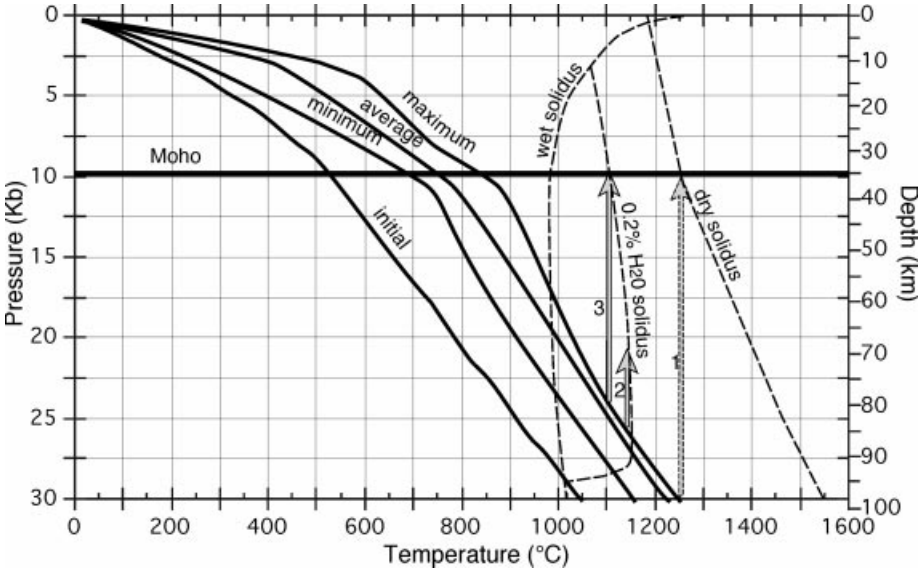

Figure 13. Shear-zone lithospheric geotherms calculated for a 4 cm yr^{-1} shear rate compared with peridotite melting curves. *Steady-state model geotherms.* Same as in Fig. 12. *Simplified upper mantle melting curves.* Wet solidus: H_20-saturated peridotite (Kushiro *et al.* 1968); dry solidus: dry peridotite solidus (Wyllie 1971); solidus for pyrolite with $\approx$0.2 per cent H_20 (Green 1973). Arrows 2 and 3 correspond to possible decompression paths leading from a shear-heating geotherm to mantle partial fusion in the case of a slightly hydrous upper mantle. Note that such decompression melting is impossible if starting from the initial geotherm.

shear zones of Brittany (e.g. Jegouzo 1980; Strong & Hanmer 1981), and Iberia (Burg et al. 1981; Reavy *et al.* 1991) are associated with synkinematic two-mica leucogranites that result from partial melting of crustal material, probably metasediments (Table 2) (Reavy *et al.* 1991; Strong & Hanmer 1981). Along the Don Féliciano transcurrent belt of Brazil, two generations of granitoids were emplaced during deformation (Tommasi *et al.* 1994): first, calc-alkaline metaluminus granodiorites to adamellites probably resulting from fluid-absent lower crustal melting; second, sodi-potassic to sodic peraluminous leucogranites that probably result from partial melting of fluid-bearing middle crust.

In orogens, crustal shortening induces the thickening and burial of the radiogenic layers. After thermal relaxation, this results in an overall heating of the crust that is regarded as responsible for regional metamorphism (e.g. England & Thompson 1984; Gaudemer *et al.* 1988). However, even in the most favourable case (instantaneous doubling of crust), thermal relaxation produce only 5 wt per cent melt in the lower crust 40 Myr after thickening (Thompson & Conolly 1995). In order to produce larger amounts of melt, mantle delamination (e.g. Houseman *et al.* 1981) is often invoked. It has been interpreted as responsible for granitoid emplacement in a strike-slip regime in the British Caledonides (Hutton & Reavy 1992). However, this mechanism would produce a thermal anomaly and melt emplacement over an area broader than the strike-slip shear zone. Furthermore, delamination can only occur after significant crustal thickening, late in the collision history. It may thus explain magmatism only in the case of late to post-orogenic strike-slip faults.

On the other hand, shear heating could explain high-temperature metamorphism and the onset of magmatism in strike-slip shear zones earlier in the collision history. Even small, because in a hot lithosphere, shear heating might induce strain localization and account for the additional heat needed to produce partial melting in thermal relaxation models. Note that shear heating in the upper mantle inducing melting of the base of the crust, rise of melts in the fault pathway and, finally, mid-crustal fusion, explains the relative timing and composition of syn-shear granites of the Don Féliciano belt (Tommasi *et al.* 1994).

5 IMPLICATIONS ON DEEP STRUCTURE OF LITHOSPHERIC FAULTS AND STRAIN LOCALIZATION

Most previous studies have considered that shear heating takes place in the brittle portion of faults only. If this were the case, near-surface high temperatures along strike-slip faults could be explained but for improbable high shear stresses, while lower crustal high-grade metamorphism and partial fusion in exhumed strike-slip shear zones would be di cult to justify. The steady-state model of a translithospheric strike-slip fault zone presented here may explain the association of deformation, metamorphism and plutonism frequently observed in ductile shear zones, without requiring shear stresses higher than several tens of megapascals in the crustal part of the fault zone.

As expected from previous theoretical calculations (Brun & Cobbold 1980; Fleitout & Froidevaux 1980; Ricard *et al.* 1983), a bu ering e ect exists as shear heating produces less heat at high temperatures. However, consideration of a two-layer medium (crust and mantle), and shear heating in both brittle and ductile regimes, limits the bu ering e ect. In particular, at temperatures for which shear heating in the soft lower crust is negligible, deformation of the strong ductile upper mantle continues to produce heat. Shear heating will be particularly strong if the fault a ects an initially cold lithosphere, if the shear rate is high, if e ective friction is high and if the crust and the mantle have hard rheologies. In favourable cases, temperatures higher than previously thought could be reached, with an absolute upper bound of $\approx$600 °C for the temperature increase.

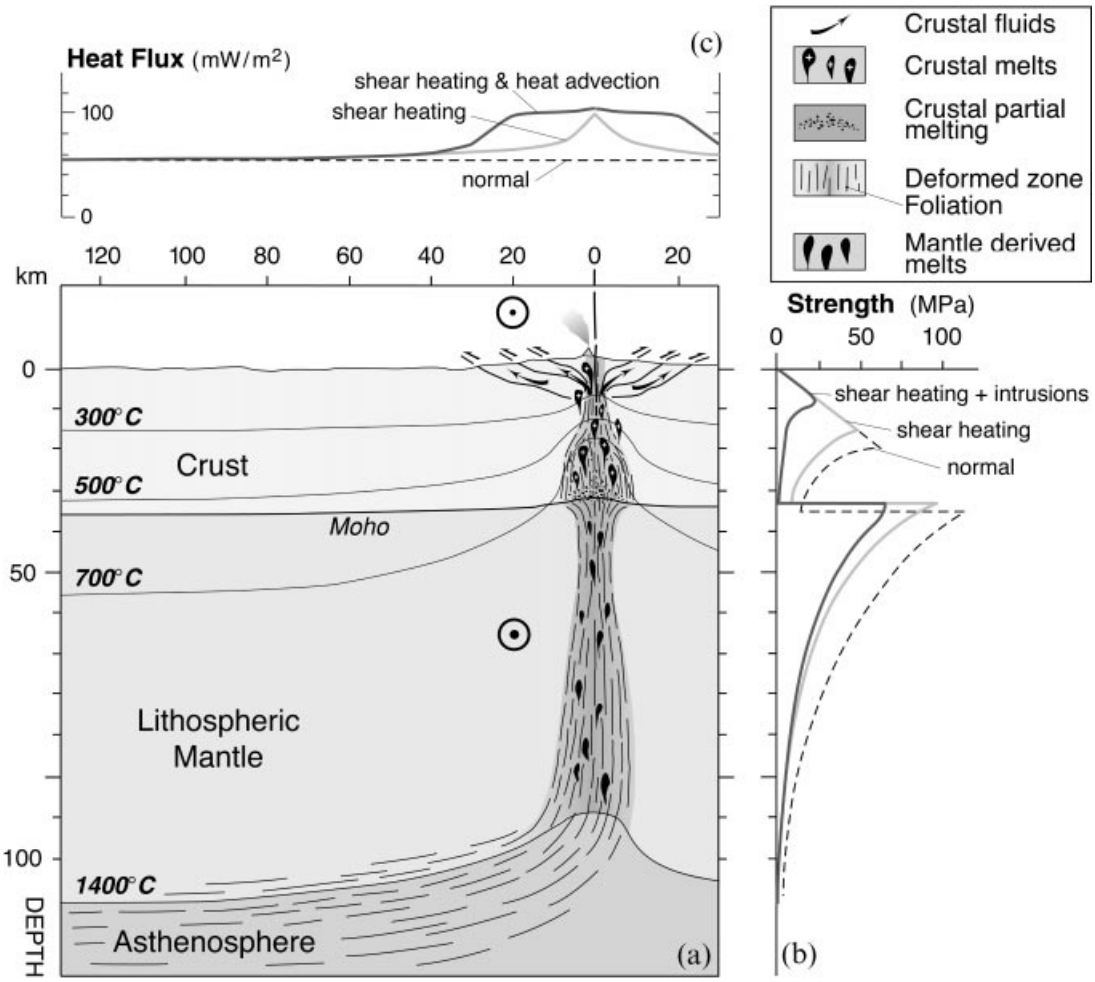

Figure 14. Sketch of a continental strike-slip fault at lithospheric scale, modified from Leloup *et al.* (1995). (a) Structure of shear zone at lithospheric scale. Because of shear heating, the 300 °C, 500 °C and 700 °C isotherms (upper limits of greenschist facies, amphibolite facies and hydrous partial melting, respectively) are shallower in the shear zone. Shear heating in the upper mantle can be strong enough to initiate partial melting of the lower crust, and hence to induce the ascent of crustal melts in the shear zone. (b) Strength profiles along shear zone for cases of: no shear heating (dashed line), shear heating and heat transport only by conduction (grey line), shear heating inducing partial melting of lower crust and heat advection in the shear zone (black line). (c) Estimates of surface heat flow across the fault for the cases in (b). Because of shear heating, heat flow is higher near the fault. The heat-flow anomaly is possibly amplified and broadened by heat advection (rise of melts in the shear zone and migration of hot fluids out of the upper crustal shear zone).

Our purely conductive model underestimates the temperatures observed in natural shear zones, leading us to infer that the fault zone is probably a good pathway for hot fluids, enhancing convective heat transport. First, this would substantially raise temperatures in the upper part of the shear zone, thus increasing both vertical and horizontal thermal gradients. Second, this e cient heat transport would extract heat from where it is produced, thus increasing the net heat production by shear. These two e ects can be particularly strong when lower-crust partial fusion occurs, possibly giving rise to the very fast ascent of magmas in the shear zone.

Melting of water-saturated rocks could occur quite easily in lithospheric shear zones, even at low shear rates ($V \approx 1$ cm yr^{-1}). In the absence of such water-saturated rocks, melting can occur by dehydration melting of muscovite and biotite at higher shear rates ($V \geq 3$ cm yr^{-1}) and for average and hard mantle rheologies. Thus, crustal thickening is unnecessary to explain the high-grade metamorphism and magmatism associated with strike-slip fault zones.

In our model, ductile deformation is not *a priori* localized, but shear heating leads to localization in a narrow shear zone a few tens of kilometres wide. This modelled shear zone is 2–3 times larger than those observed in the field. It probably implies that shear heating is not the only strain-softening mechanism. Together with the probable major e ect of melts emplaced in the shear zone, other softening mechanisms such as structural softening (rotation of structures to a more favourable orientation with respect to the stress regime, formation of a fault-parallel mylonitic anisotropy) or small-scale mechanisms (dynamic recrystallization, grain size reduction etc.) may concur to further decrease the shear-zone width and enhance strain localization.

ACKNOWLEDGMENTS

This manuscript benefited from constructive reviews by Mousumi Roy and an anonymous reviewer. We thank P. Tapponnier, G. King, S. Tait and many others for discussions

during the extended gestation of this paper. This is IPGP contribution no. 1548.

REFERENCES

Adams, J., 1979. Vertical drag on the Alpine fault, New Zealand, in *The origin of the Southern Alps*, eds Walcott, R.I. & Cresswell, M.M., *R. Soc. NZ bull.,* **18,** 47–53.

Adams, C.J. & Gabites, J.E., 1985. Age of metamorphism and uplift in the Haast schist group at Haast pass, lake Wanaka and lake Hawea, South Island, New Zealand, *NZ J. Geol. Geophys.,* **28,** 85–96.

Atwater, T. & Molnar, P., 1973. Relative motion of the Pacific and North American plates deduced from sea-floor spreading in the Atlantic, Indian and South Pacific Oceans, in *Proc. conf. tectonic problems of the San Andreas fault system*, eds Kovach, R.L. & Nur, A., *Stanford Univ. publ. geol. Sci.,* **13,** 136–148.

Barr, T.D. & Dahlen, F.A., 1989. Brittle frictional mountain building 2. Thermal structure and heat budget., *J. struct. Geol.,* **94,** 3923–3947.

Berryman, K.R., Beanland, S., Cooper, A.F., Cutten, H.N., Norris, R.J. & Wood, P.R., 1992. The Alpine fault, New Zealand variation in Quaternary structural style and geomorphic expression, *Ann. Tect.,* **6** (sup.), 126–163.

Brace, W.F. & Kohlstedt, D.L., 1980. Limits on lithospheric stress imposed by laboratory experiments, *J. geophys. Res.,* **85,** 6248–6252.

Brun, J.P. & Cobbold, P.R., 1980. Strain heating and thermal softening in continental shear zones: a review, *J. struct. Geol.,* **2,** 149–158.

Bull, W.J. & Cooper, A.F., 1986. Uplifted marine terraces along the Alpine fault, New Zealand, *Science,* **234,** 1225–1228.

Burg, J.P., Iglesias, M., Laurent, P., Matte, P. & Ribeiro, A., 1981. Variscan intracontinental deformation: the Coimbra-Cordoba shear zone (SW Iberian peninsula), *Tectonophysics,* **78,** 161–177.

Byerlee, J., 1978. Friction of rocks, *Pure appl. Geophys.,* **116,** 615–626.

Carter, N.L. & Tsenn, M.C., 1987. Flow properties of continental lithosphere, *Tectonophysics,* **136,** 27–63.

Chapman, D.S. & Furlong, K.P., 1991. Thermal state of the continental lower crust, in *Development in Geotectonics,* No. 23, eds Fountain, D.M., Arculus, R. & Kay, R.W., Elsevier.

Chen, W.P. & Molnar, P., 1983. Focal depths of intracontinental and intraplate earthquakes and their implications for the thermal and mechanical properties of the lithosphere, *J. geophys. Res.,* **88,** 4183–4214.

Chopra, P.N. & Paterson, M.S., 1981. The experimental deformation of dunite, *Tectonophysics,* **78,** 453–473.

Chopra, P.N. & Paterson, M.S., 1984. The role of water in the deformation of dunite, *J. geophys. Res.,* **89,** 7861–7876.

Cooper, A.F., Barreiro, B.A., Kimbrough, D.L. & Mattinson, J.M., 1987. Lamprophyre dike intrusion and the age of the Alpine fault, New Zealand, *Geology,* **15,** 941–944.

De Mets, C., Gordon, R.G., Argus, D.F. & Stein, S., 1990. Current plate motions, *Geophys. J. Int.,* **101,** 425–478.

Deming, D., 1994. Estimation of the thermal conductivity anisotropy of rock with application to the determination of terrestrial heat flow, *J. geophys. Res.,* **99,** 22 087–22 091.

Dickinson, W.R., 1981. Plate tectonics and the continental margin of California, in *The Geotectonic Development of California* (Rubey Vol. 1), pp. 1–28, ed. Ernst, W.G., Prentice-Hall, Englewood Cli s, NJ.

Dickinson, W.R. & Snyder, W.S., 1979. Geometry of triple junctions related to San Andreas transform, *J. geophys. Res.,* **84,** 561–572.

England, P. & Molnar, P., 1991. Inferences of deviatoric stress in actively deforming belts from simple physical models, *Phil. Trans. R. Soc. Lond.*, A, **337,** 151–164.

England, P.C. & Thompson, A.B., 1984. Pressure–temperature–time paths of regional metamorphism I. Heat transfer during the evolution of regions of thickened continental crust, *J. Petrol.,* **25,** 894–928.

Findlay, R.H., 1987. Structure and interpretation of the Alpine schists in Copland and Cook River Valleys, South island, New Zealand, *NZ J. Geol. Geophys.,* **30,** 117–138.

Fitch, T.J., 1972. Plate convergence, transcurrent faults and internal deformation adjacent to southeast Asia and the western Pacific, *J. geophys. Res.,* **77,** 4432–4460.

Fleitout, L. & Froidevaux, C., 1980. Thermal and mechanical evolution of shear zones, *J. struct. Geol.,* **2,** 159–164.

Gardien, V., Thompson, A.B., Grujic, D. & Ulmer, P., 1994. The role source composition on melt fraction generation during crustal anatexis, *EOS, Trans. Am. geophys. Un.,* **75,** 359–360.

Gary, S.F. & Mooney, W., 1990. Lithospheric structure and tectonics from seismic-refraction and other data, in *The San Andreas Fault System, California,* Chapter 8, ed. Wallace, R.E., US geol. Survey Prof. Paper, **1515,** 61–80.

Gaudemer, Y., Jaupart, C. & Tapponnier, P., 1988. Thermal control. on post-orogenic extension in collision belts, *Earth planet. Sci. Lett.,* **89,** 48–62.

Goetze, C. & Evans, B., 1979. Stress and temperature in the bending lithosphere as constrained by experimental rock mechanics, *Geophys. J. R. astr. Soc.,* **59,** 463–478.

Grapes, R.H., 1995. Uplift and exhumation of alpine schist, Southern Alps, New Zealand: thermobarometric constraints, *NZ J. Geol. Geophys.,* **38,** 525–533.

Green, D.H., 1973. Experimental melting studies on a model upper mantle composition at high pressure under water-saturated and water-undersaturated conditions, *Earth planet. Sci. Lett.,* **19,** 37–53.

Hanmer, S., 1988. Great Slave Lake shear zone, Canadian shield: reconstructed vertical profile of a crustal-scale fault zone, *Tectonophysics,* **149,** 245–264.

Hansen, F.D. & Carter, N.L., 1983. Semibrittle creep of dry and wet Westerly granite at 1000 MPa, in *Proc. Conf. 24th US symp. on rock mechanics,* pp. 429–447, Texas A&M University, College Station.

Harper, C.T. & Landis, C.A., 1967. K–Ar ages from regionally metamorphosed rocks, South Island, New Zealand, *Earth planet. Sci. Lett.,* **2,** 419–429.

Ho man, P.F., 1987. Continental transform tectonics: Great Slave Lake shear zone (ca.1.9 Ga), northwest Canada, *Geology,* **15,** 785–788.

Houseman, G., McKenzie, D. & Molnar, P., 1981. Convective instability of a thickened boundary layer and its relevance for the thermal evolution of continental convergent belts, *J. geophys. Res.,* **86,** 6115–6132.

Hutton, D.H.W. & Reavy, R.J., 1992. Strike-slip tectonics and granite petrogenesis, *Tectonics,* **11,** 960–967.

Irwin, W.P., 1990. Geology and plate-tectonic development, in *The San Andreas fault system, California*, Chapter 3, ed. Wallace, R.E., US geol. Survey Prof. Paper, **1515,** 61–80.

Jegouzo, P., 1980. The South Armorican shear zone, *J. struct. Geol.,* **2,** 39–47.

Joule, J.P., 1850. On the mechanical equivalent of heat, *Phil. Trans. R. Soc. Lond.,* **140,** 61–82.

Kamp, P.J.J., Green, P.F. & White, S.H., 1989. Fission-track analysis reveals character of collisional tectonics in New Zealand, *Tectonics,* **8,** 169–195.

Kushiro, I., Syono, Y. & Akimoto, S., 1968. Melting of a peridotite nodule at high pressures and high water pressures, *Geophys. Res. Lett.,* **73,** 6023–6029.

Lacassin, R., 1989. Plate-scale kinematics and compatibility of crustal shear zones in the Alps, in *Alpine Tectonics*, eds Coward, M.P., Dietrich, D. & Park, R.G., Geol. Soc. Spec. Publ., **45,** 339–352.

Lachenbruch, A.H. & Sass, J.H., 1980. Heat flow and energetics of the San Andreas fault zone, *J. geophys. Res.,* **85,** 6185–6222.

Le Breton, N. & Thompson, A.B., 1988. Fluid-absent (dehydration) melting of biotite in metapelites in the early stages of crustal anatexis, *Contrib. Mineral. Petrol.,* **99,** 226–237.

Leloup, P.H. & Kienast, J.R., 1993. High Temperature metamorphism in a major Tertiary ductile continental strike-slip shear zone: the Ailao Shan-Red River (P.R.C.), *Earth planet. Sci. Lett.,* **118,** 213–234.

Leloup, P.H., Lacassin, R., Tapponnier, P., Schärer, U., Zhong Dalai, Liu Xiaohan, Zhang Liangshang, Ji Shaocheng & Phan Trong Trinh, 1995. The Ailao Shan-Red River shear zone (Yunnan, China), Tertiary transform boundary of Indochina, *Tectonophysics,* **251,** 3–84.

Mc Garr, A., Zoback, M.D. & Hanks, T.C., 1982. implication of an elastic analysis of in situ stress measurements near the San Andreas fault, *J. geophys. Res.,* **87,** 7797–7806.

Molnar, P. & England, P., 1990. Temperatures, heat flux, and frictional stress near major thrust faults, *J. geophys. Res.,* **95,** 4833–4856.

Mount, V.S. & Suppe, J., 1987. State of stress near the San Andreas fault: implications for wrench tectonics, *Geology,* **15,** 1143–1146.

Nicolas, A., Bouchez, J.L., Blaise, J. & Poirier, J.P., 1977. Geological aspects of deformation in continental shear zones, *Tectonophysics,* **42,** 55–73.

O'Neil, J.R. & Hanks, T.C., 1980. Geochemical evidence for water–rock interaction along the San Andreas and Garlock faults of California, *J. geophys. Res.,* **85,** 6286–6292.

Peltzer, G., Tapponnier, P., Gaudemer, Y., Meyer, B., Guo, S., Yin, K., Chen, Z. & Dai, H., 1988. O sets of late Quaternary morphology, rate of slip, and recurrence of large earthquakes on the Changma fault (Gansu, China), *J. geophys. Res.,* **93,** 7793–7812.

Petö, P., 1976. An experimental investigation of melting relations involving muscovite and paragonite in the silica-saturated portion of the system K2O-Na2O-Al2O3-SiO2-H2O to 15kb total pressure, in *Progress in experimental petrology. Third progress report of research supported by NERC at Edinburgh and Manchester universities, publications series D,* vol. 6, pp. 41–45, ed. Biggar, G.M., NERC, London.

Pinet, C. & Jaupart, C., 1987. the Vertical distribution of radiogenic heat production in the Precambrian crust of Norway and Sweden: geothermal implications, *J. geophys. Res.,* **14,** 260–263.

Pinet, C., Jaupart, C., Mareschal, J.C., Gariepy, C., Bienfait, G. & Lapointe, R., 1991. Heat flow and structure of the lithosphere in the Eastern Canadian shield, *J. geophys. Res.,* **96,** 19 941–19 963.

Post, R.L., 1977. High-temperature creep of Mt Burnet Dunite, *Tectonophysics,* **42,** 75–110.

Raleigh, C.B., Kirby, S.H., Carter, N.L. & Avé Lallemant, H.G., 1971. Slip and the clinoenstatite transformation as competing rate processes in enstatite, *J. geophys. Res.,* **76,** 4011–4022.

Reavy, R.J., Stephens, W.E., Fallick, A.E., Halliday, A.N. & Godinho, M.M., 1991. Geochemical and isotopic constraints on granite petrogenesis: the Serra da Freita pluton, a typical granite body from the Portuguese Hercynian, *Geol. Soc. Am. Bull.,* **103,** 392–401.

Ricard, Y., Froidevaux, C. & Hermance, J.F., 1983. Model heat flow and magnetotellurics for the San Andreas and oceanic transform faults., *Ann. Geophys.,* **1,** 47–52.

Scaillet, B., Holtz, M., Pichavant, M. & Schmidt, M., 1996. The viscosity of Himalayan leucogranites: implications for mechanisms of granitic magma ascent., *J. geophys. Res.,* **101,** 27 691–27 699.

Schärer, U., Tapponnier, P., Lacassin, R., Leloup, P.H., Zhong Dalai & Ji Shaocheng, 1990. Intraplate tectonics in Asia: a precise age for large-scale Miocene movement along the Ailao Shan-Red River shear zone, China, *Earth planet. Sci. Lett.,* **97,** 65–77.

Schärer, U., Lian-Sheng, Z. & Tapponnier, P., 1994. Duration of strike-slip movements in large shear zones: the Red River belt, China., *Earth planet. Sci. Lett.,* **126,** 379–397.

Scholz, C.H., 1980. Shear heating and the state of stress on faults, *J. geophys. Res.,* **85,** 6174–6184.

Scholz, C.H., Beavan, J. & Hanks, T.C., 1979. Frictional metamorphism, argon depletion, and tectonic stress on the Alpine fault, New Zealand, *J. geophys. Res.,* **84,** 6770–6782.

Sclater, J.G., Jaupart, C. & Galson, D., 1980. The heat flow through oceanic and continental crust and the heat loss of the earth, *Rev. Geophys. Space Phys.,* **18,** 269–311.

Sheppard, D.S., Adams, C.J. & Bird, G.W., 1975. Age of metamorphism and uplift in the Alpine schist belt, New Zealand, *Geol. Soc. Am. Bull.,* **86,** 1147–1153.

Sibson, R.H., 1984. Roughness at the base of the seismogenic zone: contributing factors, *J. geophys. Res.,* **89,** 5791–5799.

Sibson, R.H., White, S.H. & Atkinson, B.K., 1979. Fault rock distribution and structure within the Alpine fault zone: a preliminary account, in *The Origin of the Southern Alps,* eds Walcott, R.I. & Cresswell, M.M., *R. Soc. NZ Bull.,* **18,** 55–65.

Sieh, K.E. & Jahns, R.H., 1984. Holocene activity of the San Andreas fault at Wallace Creek, California, *Geol. Soc. Am. Bull.,* **95,** 883–896.

Stock, J. & Molnar, P., 1987. Revised history of early Tertiary plate motion in the south-west Pacific, *Nature,* **325,** 495–499.

Strong, D.F. & Hanmer, S.K., 1981. The leucogranites of southern brittany: origin by faulting, frictional heating, fluid flux and fractional melting, *Can. Min.,* **19,** 163–176.

Tapponnier, P., Lacassin, R., Leloup, P.H., Schärer, U., Zhong Dalai, Liu Xiaohan, Ji Shaocheng, Zhang Lianshang & Zhong Jiayou, 1990. The Ailao Shan/Red River metamorphic belt: Tertiary left-lateral shear between Indochina and South China, *Nature,* **343,** 431–437.

Tapponnier, P. & Molnar, P., 1976. Slip-line field theory and large-scale continental tectonics, *Nature,* **264,** 319–324.

Tapponnier, P., Peltzer, G. & Armijo, R., 1986. On the mechanics of the collision between India and Asia, in *Collision Tectonics*, eds Coward, M.P. & Ries, A.C., Geol. Soc. Spec. Publ., **19,** 115–157.

Thatcher, W. & England, P.C., 1998. Ductile shear zones beneath strike-slip faults: implications for the thermomechanics of the San Andreas fault zone, *J. geophys. Res.,* **103,** 891–905.

Thompson, A.B., 1982. Dehydration melting of pelitic rocks and the generation of H2O-undersaturated granitic liquids, *Am. J. Sci.,* **282,** 1567–1595.

Thompson, A.B. & Conolly, A.D., 1995. Melting of the continental crust: some thermal and petrological constrains on anatexis in continental collision zones and other tectonic settings, *J. geophys. Res.,* **100,** 15 565–15 579.

Tommasi, A., Vauchez, A., Fernandes, L.A.D. & Porcher, C.C., 1994. Magma-assisted strain localization in an orogen-parallel transcurent shear zone of southern Brazil, *Tectonics,* **13,** 421–437.

Weertman, J., 1978. Creep laws for the mantle of the earth, *Phil. Trans. R. Soc. Lond.,* **288,** 9–26.

Wellman, H.R., 1955. New Zealand Quaternary tectonics, *Geol. Rund.,* **43,** 248–257.

Wellman, H.W., 1979. An uplift map for the South Island of New Zealand, and a model for uplift of the Southern Alps, in *The origin of the Southern Alps*, eds Walcott, R.I. & Cresswell, M.M., *R. Soc. NZ Bull.,* **18,** 13–20.

Wellman, H.W., 1984. The Alpine fault, New Zealand, near Milford Sound and to the southwest, *Geol. Mag.,* **121,** 437–441.

Woodward, D.J., 1979. The crustal structure of the Southern Alps, New Zealand, as determined by gravity, *R. Soc. NZ Bull.,* **18,** 95–98.

Wyllie, P.J., 1971. *The Dynamic Earth: a Text Book in Geosciences,* John Wiley & Sons, New York.

Yan Qizhong, Zhang Guoqing, Kan Rongju & Hu Hongxiang, 1985. The crust structure of Simao to Malong profile, Yunnan povince, China, *J. seism. Res.,* **8,** 249–264.

Yuen, D.A., Fleitout, L., Schubert, G. & Froidevaux, C., 1978. Shear deformation zones along major transform faults and slabs, *Geophys. J. R. astr. Soc.,* **54,** 93–120.

Zandt, G. & Furlong, K.P., 1982. Evolution and thickness of the lithosphere beneath coastal California, *Geology,* **10,** 376–381.

Zhang, L.-S., 1995. Age, durée et magmatisme du décrochement Tertiaire du Fleuve Rouge, Yunnan, Chine, *PhD thesis,* Université Paris 7, France.

Zoback, M.D. *et al.,* 1987. New evidence on the state of stress of the San Andreas of the San Andreas fault system, *Science,* **238,** 1105–1111.

APPENDIX A: FULL MODEL FORMULATION AND COMPARISON WITH SIMPLIFIED SOLUTIONS

For ductile deformation, we introduce the equivalent viscosity η, which is a function of stress and temperature:

$$\eta^{-1} = A\, \mathrm{e}^{-E/RT}(\tau_{yx}^2 + \tau_{yz}^2)^{(N-1)/2}. \quad \text{(A1)}$$

Therefore, the relationships between velocity gradients and stresses (see eqs 4 and 5) are

$$\tau_{xy} = \eta \frac{\partial V}{\partial x}, \quad \text{(A2)}$$

$$\tau_{yz} = \eta \frac{\partial V}{\partial z}. \quad \text{(A3)}$$

The viscosity can therefore be expressed as a function of the

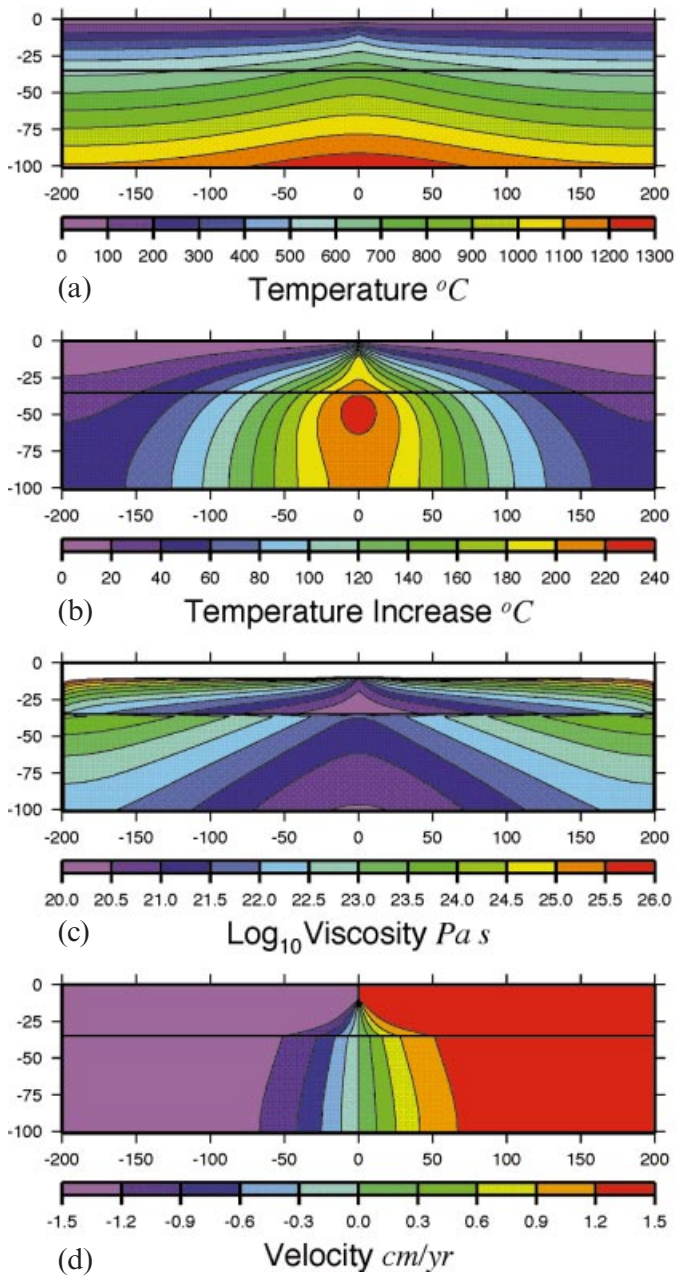

Figure A1. Full model (fine grid, exact solution) results for reference parameters. Vertical sections perpendicular to the fault (brittle fault at $x = 0$, at the left boundary of the calculation grid). Depth and distance from fault in kilometres. Depth of the brittle/ductile transition is imposed at 10 km to allow comparison with Fig. 3. (a) Final isotherms. (b) Temperature increase due to shear heating. (c) Viscosity (logarithmic scale). (d) Velocity field (in cm yr^{-1}, with respect to the main fault).

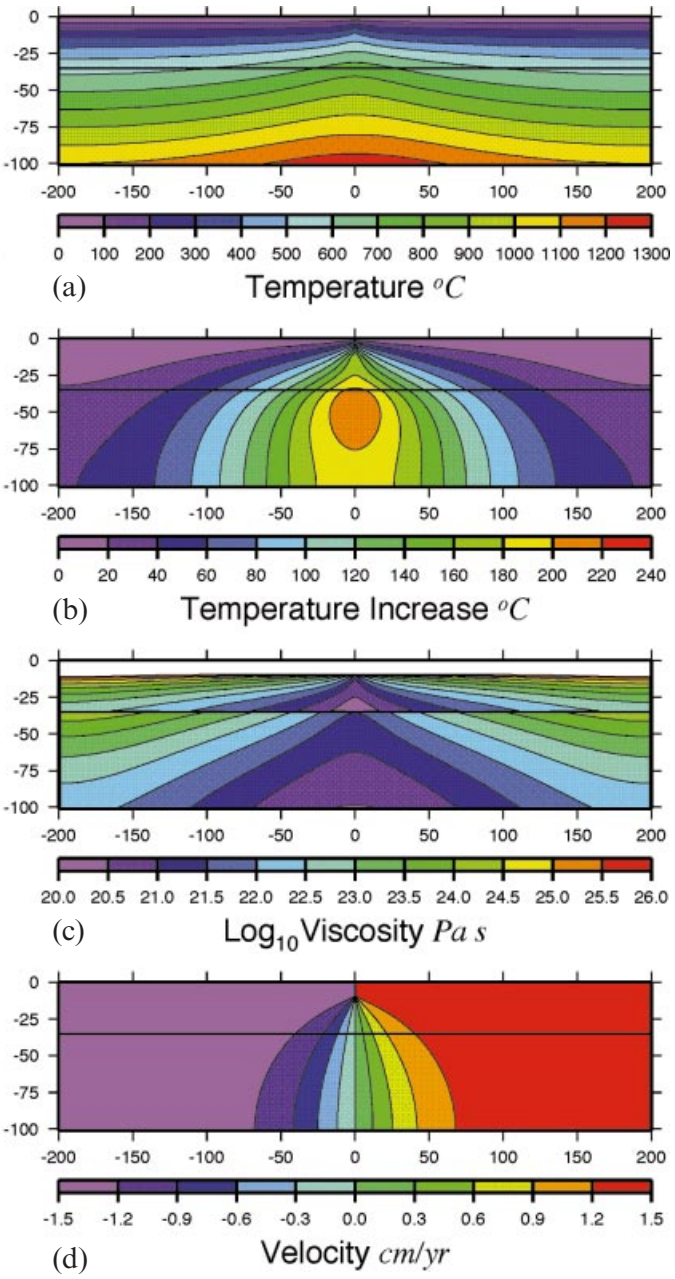

Figure A2 As Fig. A1, but neglecting shear heating on horizontal planes.

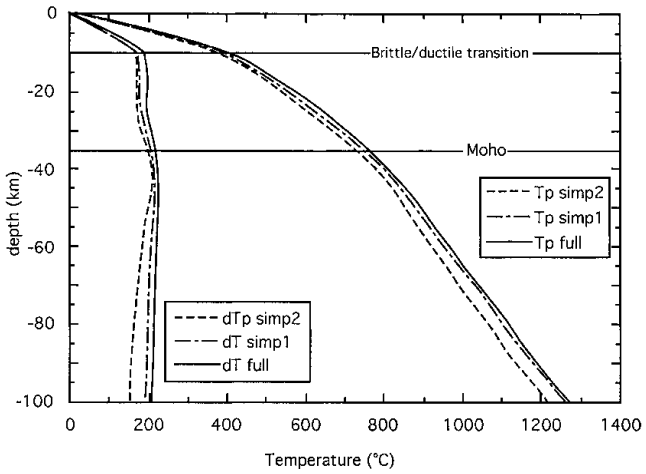

Figure A3. Comparison of results from di erent models for reference parameters, on a vertical section along the fault. Temperature increase due to shear heating (left) and final temperatures (right). Plain lines: fine grid and exact solution (full model); dot-dashed lines: fine-grid model but neglecting shear heating on horizontal planes (simplified model 1); dashed lines: coarse grid but neglecting shear heating on horizontal planes (simplified model 2).

velocity derivatives using (A1), (A2) and (A3):

$$\log \eta = \frac{E}{NRT} - \frac{\log A}{N} - \frac{N-1}{2N} \log \left[\left(\frac{\partial V}{\partial x} \right)^2 + \left(\frac{\partial V}{\partial z} \right)^2 \right]. \quad \text{(A4)}$$

This equation shows that the non-linear viscosity decreases with the local curvature of the velocity field. Note that, if $N = 1$, the rheology is linear (Newtonian material), the dependence of viscosity on velocity vanishes, and (A4) is similar to eq. (1) of Thatcher & England (1998).

The condition of mechanical equilibrium (3) thus reads

$$\nabla^2 V + \nabla(\log \eta) \nabla V = 0. \quad \text{(A5)}$$

In the ductile half-space, the steady-state heat conservation equation (12) can be expressed as

$$K \nabla^2 T + Q_r + \eta \left[\left(\frac{\partial V}{\partial x} \right)^2 + \left(\frac{\partial V}{\partial z} \right)^2 \right] = 0, \quad \text{(A6)}$$

where Q_r are the radioactive sources. In the brittle layers, the viscosity-dependent term is simply replaced by (9).

Eqs (A4), (A5) and (A6) are solved using a finite di erence algorithm on a staggered grid. Only one side of the fault is modelled, as we assume symmetry for viscosities and temperatures, anti-symmetry for velocities. As only the steady-state regime is needed, we use an explicit method which is easy to program. As first guesses we apply a Gaussian shape for the initial temperature distribution centred on the fault and a smooth continuous velocity field in the ductile layer verifying the velocity boundary conditions. From these initial conditions, the viscosity field is computed (A4), then the velocity field is updated (A5) and a new temperature field is computed (A6). We proceed iteratively until convergence. Our numerical code is slow but very robust and the final solution is independent of the initial conditions.

The boundary conditions on temperature are: $T = 20\,^\circ\mathrm{C} = 298$ K at the surface; $\partial T/\partial z = Ct$ e at the bottom; $\partial T/\partial x = 0$ on the fault and on the right side of the computation box (200 km away).

The boundary conditions on velocity are $V/2$ imposed and uniform in the brittle layer; $\partial V/\partial z = 0$ at the bottom of the model. In the ductile layer, $V = 0$ on the shear plane and $V/2$ is imposed on the right side of the computation box (200 km away).

The grid has a spacing of 500 m in both x and z and the number of grid nodes is thus 400×200. Final results for reference parameters are shown in Fig. A1.

To test the influence of the assumption leading to our simplified solution, deformation and shear heating negligible on horizontal planes, we have run the full code but neglecting shear heating on those planes. The final results for such a run for reference parameters are reported in Fig. A2. A comparison between Figs A1 and A2 shows only slight di erences. Temperature, temperature increase and viscosity cross-sections are very similar. Considering shear heating on horizontal planes only leads to slightly higher tmeperatures. In a vertical profile along the fault, the maximum di erence in final temperatures occurs at the brittle/ductile transition and never exceeds 5 per cent (Fig. A3). Vertical velocity gradients are greatest at the brittle/ductile boundary and at the Moho (Figs 3c, A1 and A2). We verified numerically that we can always neglect the shear heating on horizontal planes, whatever the viscosity contrast. This is because the shear-heating sources are related to the product of the velocity gradient with the shear stress. Large velocity gradients are associated with large viscosity drops and therefore low horizontal shears. The neglect of shear heating on horizontal planes thus appears to be a reasonable simplification.

A second test is to compare the full model (including shear heating on horizontal planes and with a dense grid) with our simplified solution (without shear heating on horizontal planes and with a coarse grid). A comparison between Fig. A1 and Fig. 3 again shows similar shapes of the final isotherms and temperature increases. However, final temperatures are lower in the simplified solution. On a vertical profile along the fault, final temperatures di er by less than 10 per cent. The most marked di erences appear below the brittle/ductile transition ($\Delta T = 36\,^\circ\mathrm{C}$), and in the lowermost lithosphere ($\Delta T = 50\,^\circ\mathrm{C}$). Our simplified solution thus leads to a slight underestimation of the shear-heating e ect.